Accepted Manuscript

Cytotoxicity of η^6-areneruthenium-based molecules to glioblastoma cells and their recognition by multidrug ABC transporters

Jaqueline Pazinato, Otávio M. Cruz, Karine P. Naidek, Amanda R.A. Pires, Eduard Westphal, Hugo Gallardo, Hélène Baubichon-Cortay, Maria E.M. Rocha, Glaucia R. Martinez, Sheila M.B. Winnischofer, Attilio Di Pietro, Herbert Winnischofer

PII: S0223-5234(18)30154-5

DOI: 10.1016/j.ejmech.2018.02.026

Reference: EJMECH 10203

To appear in: *European Journal of Medicinal Chemistry*

Received Date: 8 November 2017

Revised Date: 6 February 2018

Accepted Date: 9 February 2018

Please cite this article as: J. Pazinato, Otá.M. Cruz, K.P. Naidek, A.R.A. Pires, E. Westphal, H. Gallardo, Héè. Baubichon-Cortay, M.E.M. Rocha, G.R. Martinez, S.M.B. Winnischofer, A. Di Pietro, H. Winnischofer, Cytotoxicity of η^6-areneruthenium-based molecules to glioblastoma cells and their recognition by multidrug ABC transporters, *European Journal of Medicinal Chemistry* (2018), doi: 10.1016/j.ejmech.2018.02.026.

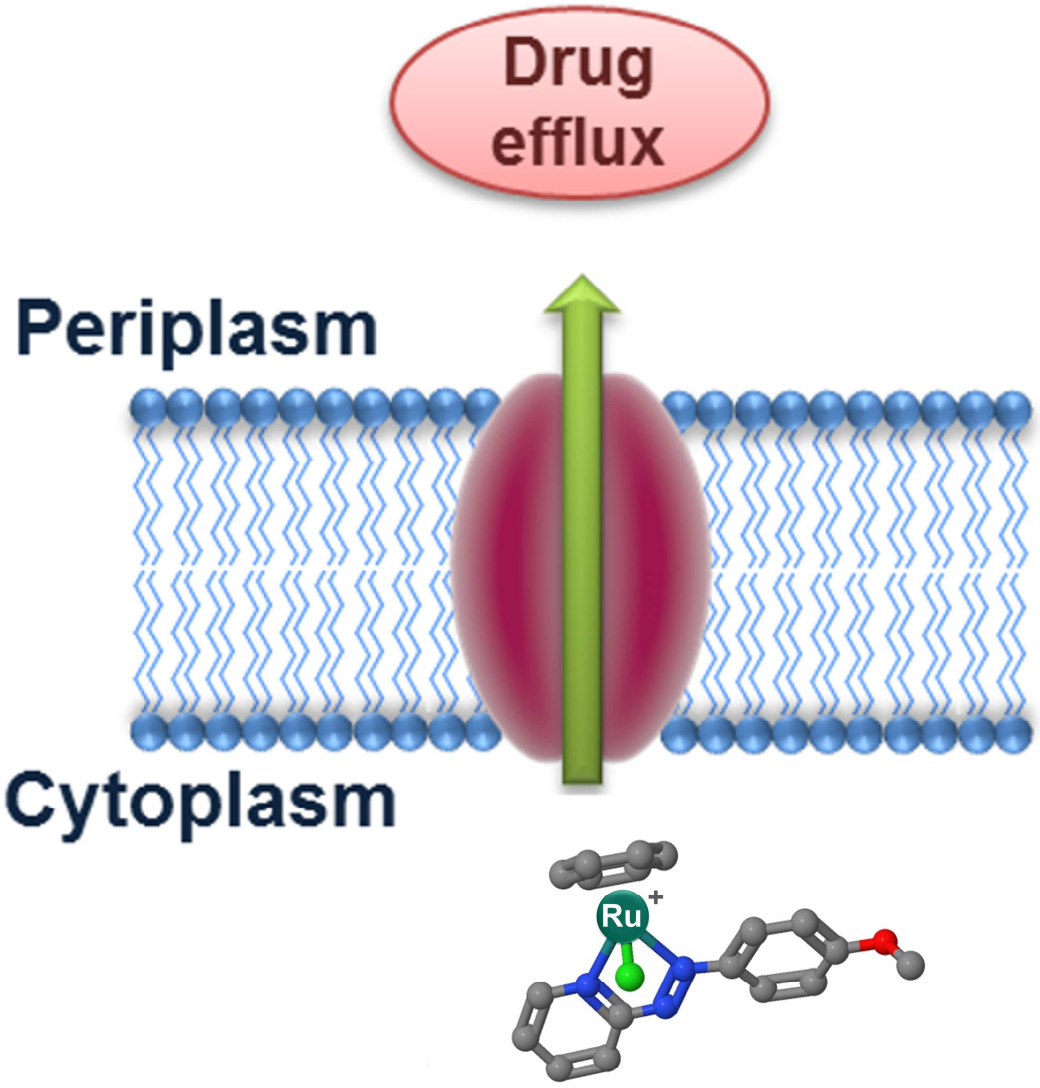

Title: Cytotoxicity of η^6-areneruthenium-based molecules to glioblastoma cells and their recognition by multidrug ABC transporters

Jaqueline Pazinato[1,5], Otávio M. Cruz[2], Karine P. Naidek[1#], Amanda R. A. Pires[2,5], Eduard Westphal[3], Hugo Gallardo[4], Hélène Baubichon-Cortay[5], Maria E. M. Rocha[2], Glaucia R. Martinez[2], Sheila M. B. Winnischofer[2], Attilio Di Pietro[5] and Herbert Winnischofer[1]**

[1] Department of Chemistry, Universidade Federal do Paraná, Curitiba, Paraná, 81531-980, Brazil

[2] Department of Biochemistry and Molecular Biology, Universidade Federal do Paraná, Curitiba, Paraná, Brazil

[3] Department of Chemistry and Biology, Universidade Tecnológica Federal do Paraná, Curitiba, Paraná, 81280-340, Brazil

[4] Department of Chemistry, Universidade Federal de Santa Catarina, Florianópolis, Santa Catarina, 88040-900, Brazil

[5] Equipe Labellisée Ligue 2014, Institut de Biologie et Chimie des Protéines, BMSSI UMR 5086, CNRS/Université Lyon 1, Lyon, France

*Corresponding authors. Tel. +55-41-3361-3181; E-mail. hwin@ufpr.br; hwin.ufpr@gmail.com (H Winnischofer); Tel. +55-41-3361-1673; E-mail. sheilambw@ufpr.br (SMB Winnischofer)

#Present address: Universidade do Estado de Santa Catarina, Centro de Ciências Tecnológicas, Joinville, Santa Catarina, 89219-710, Brazil

ABSTRACT

A new series of amphiphilic η^6-areneruthenium(II) compounds containing phenylazo ligands (group I: compounds **1a, 1b, 2a** and **2b**) and phenyloxadiazole ligands (group II: compounds **3a, 3b, 4a** and **4b**) were synthesized and characterized for their anti-glioblastoma activity. The effects of the amphiphilic η^6-areneruthenium(II) complexes on the viability of three human glioblastoma cell lines, U251, U87MG and T98G, were evaluated. The azo-derivative ruthenium complexes (group I) showed high cytotoxicity to all cell lines, whilst most oxadiazole-derivative complexes (group II) were less cytotoxic, except for compound **4a**. The cationic complexes **2a**, **2b** and **4b** were more cytotoxic than the neutral complexes. Compounds **2a** and **2b** caused a significant reduction in the percentage of cells in the G0/G1 phase, with concomitant increases in the G2/M phase and fragmented DNA in the T98G cell line. The η^6-areneruthenium(II) compounds were also tested in cell lines that overexpress the multidrug ABC transporters P-gp, MRP1 and ABCG2. Compounds **2b** and **4a** were substrates for the P-gp protein, with resistance indexes of 8.6 and 1.9, respectively. Compound **2b** was also a substrate for ABCG2 and MRP1 proteins, with lower resistance indexes (1.8 and 1.6, respectively). The contribution of multidrug ABC transporters to the cytotoxicity of compound **2b** in T98G cells was evidenced, since verapamil (a characteristic inhibitor of MRP1) increased the cytotoxicity of compound **2b** at concentrations up to 20 $\mu mol \cdot L^{-1}$, whilst GF120918 and Ko143 (specific inhibitors of P-gp and ABCG2, respectively) had no significant effect. In addition, we showed that compound **2b** interacts with glutathione (GSH), which could explain its cellular efflux by MRP1. Our results showed that the amphiphilic η^6-areneruthenium(II) complexes are promising anti-glioblastoma compounds, especially

compound **2b**, which was cytotoxic for all three cell lines, although it is transported by the three main multidrug ABC transporters.

KEYWORDS : areneruthenium, ABC transporters, multidrug resistance, glioblastoma.

1. Introduction

Glioblastoma (GBM) is one of the most aggressive forms of human astrocytoma; the median survival of patients diagnosed with GBM is 12–15 months, with approximately 5% of patients surviving for 5 years after diagnosis [1, 2]. The aggressiveness of glioma cells can be attributed to their high rates of proliferation, migration and invasion [3]. In spite of advances in various treatment regimens, such as surgical resection, external beam irradiation and chemotherapy, glioma treatments remain a significant challenge to oncologists [4]. Chemotherapy is an integral component of GBM treatment, and the major impediments to delivery of therapeutic agents to the brain include a severe toxicity, the selective permeability of the blood–brain barrier (BBB), and the presence of efflux pumps that form an insurmountable obstacle to the accumulation of drugs in the brain [5].

The multidrug resistance (MDR) phenomenon may be related to a number of factors, the main one being the resistance to drug transport across the plasma membrane, caused by increased expression of transporter proteins belonging to the ABC superfamily (ATP-binding cassette)[6, 7]. These multidrug ABC transporters use the energy generated by ATP hydrolysis to translocate a wide range of endogenous and exogenous substrates across the membrane against a sharp concentration gradient [8-11].

Currently, 48 members of the ABC transporter superfamily have been identified in humans [12-14], and three of them are involved in MDR, ABCB1 (MDR1/P-pg), ABCC1 (MRP1) and ABCG2 (BCRP). In glioma cells, overexpression of MDR1/P-glycoprotein (P-gp) and the MDR-associated protein family (MRP1–MRP9) also contributes to the

development of chemoresistance [15]. In addition, the function of the ABCG2 transporter was described in both the BBB and stem-like glioma cells [16]. Some reports suggest that in 70% of GBM cases, the intrinsic drug resistance is mostly regulated by the overexpression of MRP1 [17, 18]. Therefore, in order to improve the therapeutic effect on malignant glioma, it is essential to overcome the obstacles of the BBB and MDR.

The standard therapy for GBM includes temozolomide (TMZ) [19], an imidazotetrazine derivative, which exerts its cytotoxic effects by methylating specific DNA sites. Methylation at the O^6 position of guanine in DNA is generally considered the most critical [20], resulting in DNA fragmentation, disrupting DNA replication, and causing tumor suppression and apoptosis. Some preclinical studies have used TMZ together with cisplatin in the treatment for GBM, due to the effect of cisplatin on reducing the activity of O^6-methylguanine-DNA methyltransferase (MGMT) *in vitro* [21], suggesting a possible synergistic interaction [22, 23].

Organometallic η^6-areneruthenium(II) derivatives have been intensively investigated as potential antitumor agents [24-26], as alternatives to classical platinum complexes in cancer treatments. The η^6-areneruthenium(II) complexes have been considered to show some advantages over platinum: the amphiphilicity of the η^6-areneruthenium(II) portion due to the hydrophobic moiety on the aromatic ring, balanced by the hydrophilic metal ion, probably allows the biological compatibility and should allow easy uptake by the cells. Another important feature is the hydrolysis of the Ru-Cl bonds, forming aquaruthenium species, resulting from replacement of Cl^- by H_2O due to the low concentration of Cl^- in the cytoplasm. The aqua complexes of ruthenium are more successive for substitution than the chloride complexes [27, 28].

The prototype anticancer η^6-areneruthenium(II) complex η^6-(*p*-MeC_6H_4Pri)Ru(P-pta)Cl_2 RAPTA-C was first investigated by Allardyce et al. [29]. This compound is slightly

cytotoxic to tumor cells *in vitro* and generally free of toxicity to healthy cells, even after prolonged exposure at millimolar concentrations. However, Rapta-C is very active *in vivo*; it inhibits pulmonary metastases in CBA mice [28] and is also an antimetastatic agent [30-32]. Dougan et al. [33] reported the cytotoxic activity of η^6-areneruthenium(II) derivatives containing phenylazo ligands with activity against the A2780 ovarian and A549 lung-cancer cell lines. The authors attributed this crucial role in biological activity to the phenylazo ligand.

The present study investigated a series of eight amphiphilic η^6-areneruthenium(II) compounds, the contribution of the further hydrophobicity of the long alkyl chain, as well as the contribution of the phenylazo (group I) and phenyloxadiazole (group II) residues to the cytotoxicity in human glioma cell lines. In addition, we investigated the ability of the ruthenium complexes to be effluxed by three multidrug ABC transporters.

2. Results and discussion

2.1. Chemistry

The strategy adopted to synthesize the amphiphilic η^6-areneruthenium(II) compounds enabled us to generate charged and neutral molecules with modulated hydrophobicity. Scheme 1 illustrates the strategy used to obtain these amphiphilic complexes**.**

Scheme 1

The ESI-MS, Elemental Analysis, ^{1}H RMN and FTIR analyses gave consistent results for the molecular structure and purity for the samples. The cationic compounds **2a**, **2b**, **4a** and **4b** showed the molecular ion peak (M^+) in the ESI-MS(+) spectrum, with a characteristic isotopomeric distribution (Figures SI 1, 2, 3 and 4). On the other hand, the neutral compounds

1a, **1b**, **3a** and **3b** did not show peaks with m/z coincident with the molecular mass of the compound, but rather peaks consistent with fragments and the free ligand (Figures SI 5, 6, 7 and 8), revealing the instability of the complexes under the conditions of the experiment. In the ^{1}H NMR spectra obtained in $CDCl_3$ the chemical shifts did not show significant changes for the complexes compared to the free ligands, except for the resonance peaks assigned to the H_α and H_β of the pyridine residue of the amphiphilic ligand. Table 1 shows selected values of the chemical shifts for H_α and H_β of the complexes and free ligands (a complete description for all δ and $\Delta\delta$ values is shown in SI). For the η^6-areneruthenium(II) compounds, H_α signals were assigned to the doublet at δ = 9.3 ppm, which is 0.4–0.6 ppm up-shifted in comparison to the free ligands. The neutral compounds **1a,b** and **3a,b** exhibited the H_α signal corresponding to two equivalent hydrogens, whereas the cationic compounds **2a,b** and **4a,b** exhibited a resonance corresponding to one hydrogen only. The H_β for group I appeared as a doublet at δ = 7.67 and 7.68 ppm for **1a** and **1b**, respectively, and at δ = 7.73 and 7.76 ppm for **2a** and **2b**, respectively. The H_β for group II appeared as a doublet at δ = 7.99 ppm for **3a** and **3b**, and at δ = 7.72 and 7.75 ppm for **4a** and **4b**, respectively. For the neutral compounds, the H_β was 0.01–0.05 ppm up-shifted in comparison to the free ligands, while for the cationic compounds, this up-shift was 0.4 ppm. The benzene hydrogen signal was assigned to the singlet corresponding to six hydrogens at δ = 5.7 and 6.0–6.1 ppm for neutral and cationic complexes, respectively. The free benzene showed this resonance at δ =7.38 ppm and the precursor $Ar_2Ru_2Cl_4$ at δ = 5.95 ppm. The values of the chemical shift were affected by the aromatic ring current effect, the ruthenium(II) bonded to the N-pyridyl, and by the neighbor ligand chlorido through ruthenium bonding and through a space effect [34-36]. This last effect showed a direct relationship to the chemical shifts of the pyridine H_α and benzene H, since the resonances appeared up-shifted in compounds that have two chlorido ligands in comparison to

compounds that have only one chlorido ligand. However, H_β is more sensitive to the surroundings of the ruthenium(II) center and the azo or oxadiazo residues, in which the resonance in the compounds ranges from $\delta = 7.67$ to $\delta = 7.99$ ppm depending on the adjacent aromatic residue. These results provide evidence of the mono- or bidentated coordination of the amphiphilic ligand to the compounds. FTIR results are shown in SI (Figures SI 17, 18 and Tables SI 9 to 16). The spectra of compounds **1a ,2a, 3a** and **4a** showed bands at 3070 cm^{-1} assigned to the aromatic C-H bond, present in the benzene group; intense bands at 2920 and 2850 cm^{-1} assigned to aliphatic C-H stretching vibration, consistent with the long C_{12} chain; ~1600–1410 cm^{-1} assigned to C-N stretching vibrations present in the phenylazopyridine or phenyloxadiazolepyridine residues; and ~1025 cm^{-1} due to C-O-C stretching vibration. Compounds **1b, 2b, 3b** and **4b** showed very similar spectra, except for the absence of the aliphatic C-H stretching bands. The ionic compounds **2a,b** and **4a,b** showed an intense band associated with the νPF_6^- superimposed on the πCH vibration at 835 cm^{-1}. Usually the band frequencies up-shifted 4–10 cm^{-1} from the η^6-areneruthenium(II) compounds to the free ligands. Nevertheless the FTIR results confirmed the presence of the η^6-areneruthenium(II) portion in addition to the amphiphilic ligand. Elemental Analysis indicated the high purity of the samples, considering the ionic nature of the bidentated complexes.

Table 1

The azo- and oxadiazole- free ligands showed strong π-π^* bands under UV, which were red-shifted in the spectra of the ruthenium complexes. The azo-complexes **1a** and **1b** showed the π-π^* band at 380 nm (Figure SI 19A), whilst **2a** and **2b** showed this band at 452 nm (Figure SI 19B). The oxadiazole- complexes **3a** and **3b** showed the π-π^* band at 333 nm (Figure SI 19C). In these complexes, another π–π^* band appeared as a shoulder with maxima

below 240 nm. Exceptions were complexes **4a** and **4b**, which in addition to the π–π* band at 336 nm, showed another band at 270 nm (Figure SI 19D). The cationic bidentated complexes which the π-π* red-shifted in comparison to the neutral monodentated complexes, probably due to the additional N-binding which stabilizes the π orbitals.

The azo-derivative compounds showed the half-wave potential related to phenylazo reduction at more positive potentials than the free ligands (Figure SI20 and Table 2). This property increases the redox accessibility in biological media of the η^6-areneruthenium complexes in comparison to the free organic ligands. The cyclic voltammograms of the group I compounds (**1a**, **1b**, **2a** and **2b**) are characterized by a poorly reversible reduction process at –0.8 V for compounds **1b** and **1b** (Figure SI21) and –0.2V for compounds **2a** and **2b** (Figure 1) in acetonitrile (Fig. 1C, D). In dichloromethane, compound **2a** shows the reduction potential shifted to –0.15 V (Figure 1A). Table 2 shows peak potential values for group I compounds. Group II compounds did not undergo any redox process in the potential window analyzed. The redox process observed in the group I cyclic voltammograms is attributed to the 1 e^- reduction of the phenylazo residue to the phenylazo radical anion ({-N=N-}$^{-}$•)[37]. For compounds **2a** and **2b**, this reduction occurs at more-positive potentials than for compounds **1a** and **1b**, which agrees with the bidentated structure and cationic nature of compounds **2a** and **2b.** For compounds **2a** and **2b**, the product of this reduction is not stable and is followed by a coupled chemical reaction/transformation[33, 38]. Therefore, the product of this electrochemical/chemical reaction oxidizes at 0.1V, which is more evidenced in acetonitrile (Figure 1C, D) than in dichloromethane (Figure 1A, B).

Figure 1

Table 2

2.2. Biological evaluation

The effect of the amphiphilic η^6-areneruthenium complexes on tumor cell viability was assessed in three human GBM cell lines, U251, U87MG and T98G (Table 3). The glioma cells were treated with the η^6-areneruthenium complexes for 72 h and the cytotoxicity was measured by the MTT method. Table 2 shows the IG_{50} values (concentrations producing 50% growth inhibition) for the different compounds. The group I compounds (azo complexes) showed cytotoxic activity on all these cell lines. Compounds **2a** and **2b** were the most cytotoxic. Most compounds of group II (oxadiazole complexes) were less cytotoxic, except for compound **4a**. From the results summarized in Table 2, some tendencies could be traced: i) The phenylazo group played a special role in the cytotoxicity, since group I compounds were all cytotoxic toward the glioblastoma cell lines, while only compound **4a** in group II showed high cytotoxicity. ii) The more-hydrophobic compounds, i.e., those containing the C_{12} chain, had a tendency to be more cytotoxic than the compounds containing a methoxy group, except for the effect of compounds **1a** and **1b** on T98G cells. Increased hydrophobicity of the ligand probably facilitated cellular uptake. iii) The cationic η^6-areneruthenium(II) complexes were more cytotoxic than the neutral complexes, as shown by the IG_{50} values for **2a**, **2b** and **4a** compounds. Probably the increased amphiphilicity provided by the charged species balanced by the hydrophobic chain played a role in the cell uptake of these compounds. Palmucci *et al.* [39] described a series of neutral and cationic acylpyrazolonate η^6-areneruthenium(II) complexes with aliphatic groups in the acyl moiety, which display cytotoxicity *in vitro* against human ovarian carcinoma cells (A2780 and its resistant counterpart A2780cisR, a variant cell line with acquired resistance to cisplatin). The authors reported that complexes were highly cytotoxic to both A2780 and A2780cisR cells, and the cationic complexes bearing a long hydrophobic chain were the most cytotoxic, as seemed also to occur with our compounds.

Table 3

To evaluate whether the effects of the compounds were attributable to changes in the cell-cycle progression, we conducted DNA assays, using propidium-iodide staining and flow cytometry analysis, in permeabilized glioblastoma cells (Figure 2A and 2B). T98G cells treated with compounds **2a** and **2b** at 25 $\mu mol \cdot L^{-1}$ showed a significant reduction in the percentage of cells in the G0/G1 phase, with a concomitant increase in the G2/M phase; no change in the progression cycle was detected for the other compounds (Figure 2A). These alterations of the cell-cycle progression were intensified by treatment with compounds **2a** and **2b** at 100 $\mu mol \cdot L^{-1}$ (Figure 2B). At this higher concentration, compounds **1a**, **1b** and **4a** also caused reductions of the percentage of cells in the G0/G1 cell-cycle phase. In addition, the content of fragmented DNA in T98G cells increased after treatment with the compounds (Figure 2C). Treatment of T98G cells with compound **2a** resulted in an increase in the content of fragmented DNA at the lower concentration of 25 $\mu mol \cdot L^{-1}$. At the highest concentration (100 $\mu mol \cdot L^{-1}$), compounds **1a**, **1b**, **2a**, **2b** and **4a** also caused significant increases in fragmented DNA (Figure 1C). Taken together, the results showed that the phenylazo ruthenium compounds (group I) could alter the cell-cycle progression, with a concomitant increase in the proportion of hypodiploid cells, a hallmark of the late stage of apoptosis. These alterations were also observed for compound **4a**, the most cytotoxic compound in group II.

Figure 2

Some cell mechanisms can be associated with glioma chemoresistance, including overexpression of multidrug ABC transporters, which promotes the efflux of antitumor drugs

from the cell, thus decreasing their therapeutic effects. To elucidate whether ABC transporters played a role in the differential cytotoxic effect of these η^6-areneruthenium(II) compounds, we investigated whether these compounds were specifically toxic to cells overexpressing ABC transporters such as P-gp, MRP1, and ABCG2. Essentially, the compounds that were transported showed higher IG_{50} values for resistant cells (ABC transporter-overexpressing cells) than for the parental cell lines. The resistance index (*RI*) was calculated to determine the degree of acquired resistance of each cell line to its selective compound. *RI* was calculated from the following equation: $RI = IG_{50}$ resistant cell/IG_{50} parental cell. An *RI* value > 1.0 indicates the ability of the particular ABC transporter to confer resistance to a compound.

For the η^6-areneruthenium(II) compounds belonging to group I, compounds **1a, 1b** and **2a** were not substrates for the multidrug ABC transporters studied here (Table 4). In addition, the group II compounds **3a**, **3b** and **4b** were neither substrates for the multidrug ABC transporters (Table 4) nor highly cytotoxic (IG_{50} > 100) for all cell lines analyzed (healthy and tumor cell lines) (Table 3). However, compound **2a** showed high cytotoxic activity both for the parental cell lines (NIH 3T3, HEK 293 and BHK21) and for their resistant counterparts (Table 4). This compound was the most cytotoxic compound for the glioblastoma cell lines (Table 3). In contrast, compounds **2b** and **4a** were substrates for P-gp, with resistance indexes of 8.6 and 1.9 respectively. Compound **2b** was also a substrate for ABCG2, with a resistance index of 1.8 (Tables 4 and 5). Both compounds are cationic, which agrees with the previous observation that P-gp and ABCG2 promote a phenotype of resistance to cationic compounds [40]. Despite their efflux, compounds **2b** and **4a** retained cytotoxicity for all the glioblastoma cell lines analyzed (Table 3). Compound **2b** was also a substrate for MRP1, with a resistance index of 1.6 (Tables 4 and 5). The dynamics of transport of compound **2b** is shown in Figure 3.

Table 4

Table 5

Figure 3

To prove that compound **2b** indeed acts as a substrate for the three ABC transporters, we performed additional experiments by using selective inhibitors for P-gp (GF120918/elacridar) and ABCG2 (Ko143) and a specific cell line expressing an inactive mutant MRP1 (BHK21-MRP1m). The cytotoxic properties of compound **2b** were evaluated both in the parental cell lines (NIH 3T3, HEK 293 and BHK21) and in their resistant counterparts (NIH-P-gp, HEK-ABCG2 and BHK-MRP1m). As shown in Figure 3A, B and C, the use of the selective inhibitors or the inactive mutant cell line abolished the resistance phenotype (*RI* index almost = 1).

It is well established that MRP1 is constitutively overexpressed in cells derived from astrocytomas and glioblastomas [41]. Inhibition of MRP1 had a significant effect on the response of GBM cells to chemotherapeutics in both primary and recurrent GBM cells [42]. In the glioma cell model, the T98G cell line was reported to express high levels of P-gp and MRPs [15]. Here, the cytotoxicity analyses showed different IG_{50} values among the different cells for compound **2b**, with T98G cells displaying the highest IG_{50} (37.13 $\mu mol \cdot L^{-1}$) in comparison to the other glioblastoma cell lines analyzed (U87MG cells: IG_{50} = 4.90 $\mu mol \cdot L^{-1}$; U251 cells: IG_{50} = 8.03 $\mu mol \cdot L^{-1}$). This result can be explained by the high expression of MRP1 mRNA in T98G cells, whereas the U251 and U87MG cells had a low expression [15].

It has been established that the MRP1 protein transports only anionic compounds. Therefore, it is likely that the cationic compound **2b** needs to be converted into a conjugated anion, to enable its efflux by MRP1. One possible explanation is its interaction with glutathione (GSH), since MRP1 [43, 44] is often associated with high levels of GSH, which is the most-abundant

antioxidant species present in the cell. As it is constituted by a tripeptide (γ-Glu-Cys-Gly), GSH is negatively charged at physiological pH. GSH is often involved in detoxification processes through conjugated species [29]. Cole et al. [44] reported the role of MRP1 in transporting GSH and GSH conjugates with drugs.

In the electrochemical characterization described above, we observed the reduction process attributed to the 1 e^- reduction of the phenylazo residue to the phenylazo radical anion ({-N=N-}$^{-}$•) at E_{cp} = –0.2 V for compounds **2a** and **2b**. Once the reduction-potential value is close to the oxidation potential of GSH to disulfide-glutathione (GSSH), compounds **2a** or **2b** could react directly with GSH, promoting its oxidation. The ratio of the amounts of GSSG/2GSH mainly determines the redox state of a cell, since it determines the redox potential of the GSSG/2GSH pair. According to Schafer et al. [45] the ratio of GSSG/2GSH correlates with the biological state of the cell; cells in the proliferation stage contain a large amount of GSH and E ~ –240 mV; whereas, differentiating cells have an E ~ –200 mV; and decreases in GSH with increases in the GSSG/2GSH ratio (E ~ –170 mV) induce apoptosis. Therefore, compounds **2a** and **2b** should be able to cause an imbalance in the redox state of the cell and initiate a set of cell signals, leading to apoptosis. This could explain the cytotoxicity of these compounds.

Dougan et al. [33] reported that azopyridine-based η^6-areneruthenium(II) complexes have the ability to catalyze GSH oxidation, through a mechanism that involves an intermediate resulting from N=N bond reduction, followed by glutathione disulfide formation. To obtain more insight, we investigated the interaction between compound **2b** and GSH by UV-vis spectroscopy. Figure 4 shows a 10 mmol·L^{-1} GSH solution spectrum (black line) that shows a strong band absorption at 290 nm. After 10 s, the solution of GSH with compound **2b** showed the blue line spectrum illustrated in Figure 4, where, in addition to the GSH band at 290 nm, the compound **2b** π–π* band appears at 440 nm. After 1 h (Figure 4, red line), the 290-nm

GSH band vanished and the absorption below 250 nm increased. These changes are similar to what occurred when GSH was treated with one equivalent of hydrogen peroxide (Figure 4, dashed black line). The 440 nm π–π* band was up-shifted to 410 nm, revealing that **2b** was modified in the solution, possibly through changes in the coordination sphere of the ruthenium center. Probably the ruthenium complex undergoes solvolysis and some of the ligands are substituted. However, the 410-nm maximum is not consistent with the free azopyridine ligand, indicating that this amphiphilic ligand is still bonded to the ruthenium complex. Some of the species produced during the catalytic process of GSH oxidation should be effluxed, which could explain why **2b** is a substrate of MRP1. After 48 h, the solution of GSH and compound **2b** produced a spectrum similar to that observed after 1 h, but with a further increased band below 250 nm (data not shown). These results are consistent with the catalytic oxidation of GSH by compound **2b**.

Figure 4

To assess the functional role of multidrug ABC transporters in the cytotoxicity of compound **2b** in glioma models, T98G cells were treated with increasing concentrations of compound **2b** in the absence or in the presence of modulators of P-gp (GF120918), MRP1 (verapamil) and ABCG2 (MBLII 141 and Ko143). We found that verapamil further increased the cytotoxicity of compound **2b**. On the other hand**,** MBLII 141 showed a small effect at 2.5 $\mu mol \cdot L^{-1}$, whereas GF120918 and Ko143 produced no significant effect on the cytotoxicity of compound **2b** (Figure 5).

Despite the cationic nature of compound **2b**, we did not observe significant changes in its cytotoxicity to these cell lines in the presence of the selective inhibitor GF120918. Again, this result can be explained by conversion of **2b** into anionic species by interaction with GSH,

since T98G cells are rich in GSH; T98G cells contain 450 nmol of GSH per mg of protein, a larger amount than in other cell lines such as BHK-21 or HeLa cells [46].

Figure 5

Summarizing, we demonstrated that compounds belonging to group I were all cytotoxic to glioma cell lines, whereas only compound **4a** from group II exhibited high cytotoxicity. The more-hydrophobic compounds containing long-alkyl-chain ligands tended to be more cytotoxic than compounds having a short methoxy group. The cationic η^6-areneruthenium(II) compounds were more cytotoxic than the neutral compounds. This cytotoxicity was attributable to alterations of cell-cycle progression and increased contents of fragmented DNA, suggesting an apoptotic mechanism. Two compounds were substrates for the multidrug ABC transporters: compound **2b** (for P-gp, ABCG2 and MRP1) and **4a** (for P-gp). Specifically, for compound **2b**, in addition to being a substrate for the three transporters studied here, this compound was also cytotoxic for the glioblastoma cell lines. We showed that compound **2b** interacts with GSH. This constitutes a possible explanation of its efflux by MRP1 and its cytotoxic effect, which was further increased in the presence of verapamil in the T98G cells. In contrast, compound **2a** showed high cytotoxicity to the glioblastoma cell lines, and it was not a substrate for the transporters studied here. In conclusion, we showed that compounds **2a** and **2b** are promising for glioblastoma treatments. Further investigations are required to better understand their mechanism in the tumor cells.

EXPERIMENTAL SECTION

Characterization of the compounds

All the reagents and solvents were of analytical grade and were purchased from commercial sources (Merck, Sigma-Aldrich, Fluka, and Acros) and used as received. A Perkin-Elmer 2400 Series II CHN Elemental Analyzer was used to characterize the composition of the samples. ^{1}H NMR spectra were recorded at 298K using a Varian Mercury Plus spectrometer operating at 400 MHz, or a Bruker DPX 200 MHz spectrometer operating at 200 MHz. Deuterated chloroform ($CDCl_3$) or deuterated DMSO (DMSO-d_6) was used as the solvent and TMS as the internal standard. The mass spectra (ESI-MS) were obtained in a Thermo Fisher Scientific LTQ XL Linear Ion Trap Mass Spectrometer, using sample solutions at a concentration of 10^{-2} mg mL^{-1} in dichloromethane. High-Resolution Mass Spectra were recorded in a Bruker micrOTOF-Q II mass spectrometer, using an APPI ionization source. A Bruker Vertex 70 spectrophotometer was used to acquire FTIR spectra of the compounds embedded in KBr pellets, in the range of 400 to 4000 cm^{-1}. An Agilent 8453 or Shimadzu UV 2401 PC spectrophotometer was used to acquire the UV-vis spectra of the compounds in chloroform solutions. For GSH studies, the UV-vis spectrum of compound **2b** at 100 µM with 10 mmol·L^{-1} GSH in DMSO added, was monitored over 48 h. The GSH was oxidized to GSSH by addition of H_2O_2 at 10 mmol·L^{-1}. The electrochemical experiments were performed on an Ivium Compactstat potentiostat/galvanostat in a three-electrode cell; Ag/Ag^{+} (0.01 mol·L^{-1} in acetonitrile) reference electrode, platinum disc (diameter 3 mm) working electrode and a stainless-steel counter electrode. Experiments were conducted in 0.1 mol·L^{-1} $TBAClO_4$ electrolyte solution in dichloromethane or acetonitrile (depending on the solubility of the compound)**.**

Scheme 2

4-(4-dodecyloxyphenylazo)pyridine (L1a). The synthesis of this ligand was described in a previous paper from our group [47].

2-Hydrazinepyridine (6). A mixture of 2-chloropyridine 2.00 g (17.6 mmol) and 12 mL hydrazine monohydrate (65%) was added to a 25-mL round-bottom flask and stirred under reflux for 7 h. After this period, the solution was cooled and the product extracted with diethyl ether (2 × 20 mL). The organic phase was dried over anhydrous Na_2SO_4, filtered, and stored in a freezer. The resulting precipitate was collected by filtration and used in the next step without further purification. m.p.: 41.8–44.3 °C (lit. 45 °C) [48]. ^{1}H NMR (200 MHz, $CDCl_3$) δ ppm: 3.81 (broad, 2H, -NH_2), 6.12 (broad, 1H, -NH-), 6.67 (m, 2H, Py-H), 7.46 (ddd, *J* = 8.5 Hz, 7.1 Hz and 1.8 Hz, 1H, Py-H), 8.10 (m, 1H, Py-H).

2-(4-hydroxyphenylazo)pyridine (7). 1.27 g (11.8 mmol) hydroquinone, 8 mL sulfuric acid and 100 mL distilled water were added to an Erlenmeyer flask. To this solution and under strong stirring, 2-hydrazinepyridine (**6**) dissolved in 20 mL water was added dropwise, and the reaction mixture was stirred at room temperature for a further 90 min. The pH was adjusted to ≈ 6 using NaOH aqueous solution (20%), and the resulting precipitate was filtered and washed with distilled water. The crude product was purified by recrystallization from isopropanol/water, affording 1.95 g (83%) of the desired azo compound after the two-step procedure. m.p.: 232 °C (decomposition). ^{1}H NMR (400 MHz, DMSO-d_6) δ ppm: 6.87 (d, *J* = 8.6 Hz, 2H, Ar-H), 7.50 (m, 1H, Py-H), 7.65 (d, *J* = 8.2 Hz, 1H, Py-H), 7.87 (d, *J* = 8.6 Hz, 2H, Ar-H), 7.99 (m, 1H, Py-H), 8.67 (d, *J* = 4.4 Hz, 1H, Py-H), 10.50 (broad, 1H, -OH). ^{13}C NMR (100.6 MHz, DMSO-d_6) δ ppm: 112.86, 116.10, 124.93, 125.53, 138.67, 145.19, 149.18, 161.90, 163.13.

5-(4-dodecyloxyphenyl)tetrazole (9). This compounds was prepared by a two-step synthesis according to a previously described procedure [49].

2-(4-dodecyloxyphenylazo)pyridine (L2a). In a 100-mL round-bottom flask were added 1.40 g (7.03 mmol) 2-(4-hydroxyphenylazo)pyridine (**7**), 1.84 g (7.38 mmol) 1-bromododecane, 1.94 g (14.1 mmol) K_2CO_3 and 40 mL butanone. The reaction mixture was refluxed under stirring for 24 h, cooled to room temperature, filtered, and washed with butanone. The crude product obtained after removal of the solvent was purified by column chromatography using silica and CH_2Cl_2 as eluent, affording 2.43 g (94%) of an orange solid. m.p.: 79.0 – 79.9 °C. ^{1}H NMR (400 MHz, $CDCl_3$) δ ppm: 0.88 (t, *J* = 6.6 Hz, 3H, CH_3), 1.21 – 1.41 (m, 16H, -CH_2-), 1.47 (m, 2H, -CH_2-), 1.82 (m, 2H, -CH_2CH_2O-), 4.05 (t, *J* = 6.6 Hz, 2H, -CH_2O-), 7.01 (d, *J* = 9.0 Hz, 2H, Ar-H), 7.36 (m, 1H, Py-H), 7.79 (d, *J* = 8.2 Hz, 1H, Py-H), 7.87 (m, 1H, Py-H), 8.05 (d, *J* = 9.0 Hz, 2H, Ar-H), 8.71 (d, *J* = 4.7 Hz, 1H, Py-H). ^{13}C NMR (100.6 MHz, $CDCl_3$) δ ppm: 14.09, 22.65, 25.96, 29.11, 29.31, 29.33, 29.52, 29.55, 29.60, 29.62, 31.88, 68.40, 114.71, 115.17, 124.56, 125.69, 138.16, 146.66, 149.40, 162.68, 163.11. Q-TOF/MS for $C_{23}H_{34}N_3O$ $[M^+H]^+$: Calculated: 368.2696; Found: 368.2690.

2-(4-dodecyloxyphenyl)-5-(4-pyridyl)-1,3,4-oxadiazole (L3a). In a round-bottom flask equipped with a condenser and a drying tube ($CaCl_2$), 0.60 g (4.88 mmol) isonicotinic acid (**8**), 1 drop DMF and 5 mL $SOCl_2$ were added and refluxed for 3 h. After this period, the remaining unreacted $SOCl_2$ was removed by vacuum distillation, and 1.77 g (5.36 mmol) 5-(4-dodecyloxyphenyl)tetrazole (**9**) and 15 mL anhydrous pyridine were added to the round-bottom flask and refluxed for a further 20 h. The solution was then cooled to room temperature, poured into a 300-mL ice/water bath and basified to pH ≈ 12 with a NaOH aqueous solution (10%). The precipitate was separated by filtration, washed with water, and

recrystallized from isopropanol/H_2O solution, affording 1.75 g (88%) of a white solid. m.p: 94.8–95.4 °C. ^{1}H NMR (400 MHz, $CDCl_3$) δ ppm: 0.87 (t, *J* = 6.8 Hz, 3H, -CH_3), 1.22-1.41 (m, 16H, -CH_2-), 1.47 (m, 2H, -CH_2-), 1.82 (m, 2H, -CH_2CH_2O-), 4.03 (t, *J* = 6.5 Hz, 2H, -OCH_2-), 7.02 (d, *J* = 8.8 Hz, 2H, Ar-H), 7.97 (d, *J* = 6.0 Hz, 2H, Py-H), 8.06 (d, *J* = 8.8Hz, 2H, Ar-H), 8.82 (d, *J* = 6.0 Hz, 2H, Py-H). ^{13}C NMR (100.6 MHz, $CDCl_3$) δ ppm: 14.10, 22.66, 25.96, 29.07, 29.32, 29.34, 29.53, 29.56, 29.61, 29.63, 31.89, 68.33, 115.08, 115.42, 120.20, 128.91, 131.19, 150.77, 162.19, 162.39, 165.50. QTOF/MS for $C_{25}H_{34}N_3O_2$ $[M^+H]^+$: Calculated: 408.2646; Found: 408.2640.

2-(4-dodecyloxyphenyl)-5-(2-pyridyl)-1,3,4-oxadiazole (L4a). Under argon atmosphere, 0.80 g (6.50 mmol) picolinic acid (**10**), 2.15 g (6.50 mmol) 5-(4-dodecyloxyphenyl)tetrazole (**11**), 0.08 g (0.65 mmol) DMAP and 40 mL anhydrous toluene were added to a 100-mL Schlenk flask. After 10 min, 1.60 g (7.80 mmol) DCC was added, with an additional 10 mL toluene. The mixture was stirred for 10 min at room temperature and for 6 h at 100 °C. The reaction mixture was cooled to room temperature and 40 mL ethyl acetate was added. The precipitate was filtered, washed with ethyl acetate, and the solvent of the combined organic phases removed under reduced pressure. The crude product was purified by column chromatography using silica and a mixture of CH_2Cl_2: ethyl acetate (gradient from 100:0 to 95:5) as eluent. A final recrystallization from heptane afforded 2.07 g (78%) of a white solid. m.p.**:** 100.7–101.5 °C. ^{1}H NMR (400 MHz, $CDCl_3$) δ ppm: 0.87 (t, *J* = 6.8 Hz, 3H, -CH_3), 1.17–1.38 (m, 16H, -CH_2-), 1.46 (m, 2H, -CH_2-), 1.80 (m, 2H, -CH_2CH_2O-), 4.02 (t, *J* = 6.5 Hz, 2H, -OCH_2-), 7.00 (d, *J* = 9.0 Hz, 2H, Ar-H), 7.45 (ddd, *J* = 7.8 Hz, 4.9 Hz and 1.2 Hz, 1H, Py-H), 7.88 (ddd, *J* = 7.8 Hz, 7.8 Hz and 1.8 Hz, 1H, Py-H), 8.13 (d, *J* = 9.0 Hz, 2H, Ar-H), 8.29 (ddd, *J* = 7.8 Hz, 1.2 Hz and 1.0 Hz, 1H, Py-H), 8.80 (ddd, *J* = 4.9 Hz, 1.8 Hz and 1.0 Hz, 1H, Py-H). ^{13}C NMR (100.6 MHz, $CDCl_3$) δ ppm: 14.10, 22.65, 25.96, 29.08, 29.32,

29.52, 29.55, 29.60, 29.62, 31.88, 68.24, 114.89, 115.71, 123.06, 125.57, 129.05, 137.14, 143.75, 150.19, 162.18, 163.33, 165.58. Q-TOF/MS for $C_{25}H_{34}N_3O_2$ $[M^+H]^+$: Calculated: 408.2646; Found: 408.2644.

Scheme 3

4-(4-hydroxyphenylazo)pyridine (12). The synthesis of this compound was described in a previous report, and can be found in reference [47].

4-(4-methoxyphenylazo)pyridine (L1b). A mixture of 4-(4-hydroxyphenylazo)pyridine (**12**) 1.50 g (7.53 mmol), iodomethane 0.56 mL (9.04 mmol), K_2CO_3 2.08 g (15.06 mmol) and 50 mL acetone was added to a round-bottom flask and stirred at 50 °C for 20 h. After this period, the suspension was filtered and the solid was washed with hot methanol. The solvent was removed under reduced pressure and the product was purified by column chromatography using silica and a mixture of CH_2Cl_2:ethyl acetate (95:5) as eluent, affording 0.81 g (50%) of an orange solid. m.p.: 96.2–97.8 °C. ^{1}H NMR (200 MHz, $CDCl_3$) δ ppm: 3.91 (s, 3H, -OCH_3), 7.03 (d, *J* = 9.3 Hz, 2H, Ar-H), 7.67 (d, *J* = 6.1 Hz, 2H, Py-H), 7.97 (d, *J* = 9.3 Hz, 2H, Ar-H), 8.78 (d, *J* = 6.1 Hz, 2H, Py-H). ^{13}C NMR (50.3 MHz, $CDCl_3$) δppm: 55.64, 114.37, 116.12, 125.55, 146.80, 151.18, 157.37, 163.19. Q-TOF/MS for $C_{12}H_{12}N_3O$ $[M+H]^+$: Calculated: 214.0975; Found: 214.0978.

2-(4-hydroxyphenylazo)pyridine (7). The synthesis of this compound was described above in scheme 2.

2-(4-methoxyphenylazo)pyridine (L2b). In a round-bottom flask, 1.540 g (7.53 mmol) 2-(4-hydroxyphenylazo)pyridine (**7**), 0.56 mL (9.04 mmol) iodomethane, 2.08 g (15.06 mmol) K_2CO_3 and 100 mL acetone were added. The mixture was heated to 50 °C and stirred for 20

h. After this, the mixture was cooled to room temperature, filtered, and the solid washed with CH_2Cl_2. The crude product obtained after removal of the solvent was purified by column chromatography using silica and a mixture of CH_2Cl_2:ethyl acetate (95:5) as eluent, affording 0.85 g (53%) of an orange solid. m.p.: 49.5–51.1 °C (lit. 51–52 °C) [50]. ^{1}H NMR (200 MHz, $CDCl_3$) δ ppm: 3.91 (s, 3H, -OCH_3), 7.03 (d, *J* = 9.3 Hz, 2H, Ar-H), 7.33–7.41 (m, 1H, Py-H), 7.76–7.94 (m, 2H, Py-H), 8.07 (d, *J* = 9.3 Hz, 2H, Ar-H), 8.70–8.74 (m, 1H, Py-H). ^{13}C NMR (50.3 MHz, $CDCl_3$) δ ppm: 55.61, 114.29, 115.23, 124.64, 125.70, 138.21, 146.88, 149.44, 163.02, 163.11. Q-TOF/MS for $C_{12}H_{12}N_3O$ $[M+H]^+$: Calculated: 214.0975; Found: 214.0976.

5-(4-pyridyl)tetrazole (14). The synthesis of this compound is described in reference [51].

2-(4-methoxyphenyl)-5-(4-pyridyl)-1,3,4-oxadiazole (L3b). In a round-bottom flask equipped with a condenser and a drying tube ($CaCl_2$), 1.48 g (9.75 mmol) *p*-anisic acid (**15**), 1 drop DMF and 5 mL $SOCl_2$ were added, heated to 60 °C and stirred for 16 h. After this period, the remaining $SOCl_2$ was removed by vacuum distillation, resulting in the crude acid chloride (**16**). To the round-bottom flask, 1.43 g (9.75 mmol) 5-(4-pyridyl)tetrazole (**14**) and 15 mL anhydrous pyridine were added and the mixture refluxed for a further 24 h. The solution was then cooled to room temperature, poured into 150 mL ice/water, and the precipitate separated by filtration. The crude product was purified by column chromatography using silica and a gradient of CH_2Cl_2:ethyl acetate (from 100:0 to 90:10) as eluent. The product was further recrystallized over ethanol, affording 1.95 g (79%) of a white solid. Mp: 192.3–192.8 °C (lit. 188 °C) [52]. ^{1}H NMR (200 MHz, $CDCl_3$) δ ppm: 3.90 (s, 3H, -OCH_3), 7.04 (d, *J* = 9.0 Hz, 2H, Ar-H), 7.97 (d, *J* = 6.1 Hz, 2H, Py-H), 8.09 (d, *J* = 9.0 Hz, 2H, Ar-H), 8.83 (d, *J* = 6.1 Hz, 2H, Py-H). ^{13}C NMR (50.3 MHz, $CDCl_3$) δ ppm: 55.45, 114.57, 115.68, 120.13, 128.88, 131.06, 150.75, 162.20, 162.69, 165.35. Q-TOF/MS for $C_{14}H_{12}N_3O_2$ $[M+H]^+$: Calculated: 254.09240; Found: 254.09239.

5-(2-pyridyl)tetrazole (18). In a round-bottom flask equipped with a condenser, 5.00 g (48.1 mmol) 2-cyanopyridine (**17**), 9.37 g (144.1 mmol) NaN_3, 7.71 g (144.1 mmol) NH_4Cl and 20 mL DMF were added, heated to 130 °C, and stirred for 24 h. The suspension was cooled to room temperature, poured into 200 mL water/ice, and the pH adjusted to 6 with HCl (10%). The precipitate formed was separated by filtration and recrystallized over water, affording 5.16 g (73%) of colorless crystals. m.p.: 214.4–216.0 °C (lit. 213 °C) [53]. ^{1}H NMR (200 MHz, DMSO-d_6) δ ppm: 7.55–7.64 (m, 1H, Pyr-H), 8.00–8.09 (m, 1H, Pyr-H), 8.17–8.23 (m, 1H, Pyr-H), 8.72–8.81 (m, 1H, Pyr-H). ^{13}C NMR (50.3 MHz, DMSO-d_6) δ ppm: 122.63, 126.10, 138.23, 143.69, 150.06, 154.78

2-(4-methoxyphenyl)-5-(2-pyridyl)-1,3,4-oxadiazole (L4b). In a round-bottom flask equipped with a condenser and a drying tube ($CaCl_2$), 1.50 g (9.86 mmol) *p*-anisic acid (**15**), 1 drop DMF and 5 mL $SOCl_2$ were added, heated to 60 °C, and stirred for 16 h. After this period, the remaining $SOCl_2$ was removed by vacuum distillation, resulting in the crude acid chloride (**16**). To the round-bottom flask, 1.45 g (9.86 mmol) 5-(2-pyridyl)tetrazole (**18**) and 15 mL anhydrous pyridine were added and the mixture refluxed for a further 24 h. The solution was then cooled to room temperature, poured into 150 mL ice/water, and the product extracted with ethyl acetate (3 × 50 mL). The solvent of the combined organic phases was removed under reduced pressure and the product purified by column chromatography using silica and CH_3Cl as eluent. The product was further recrystallized over ethanol, affording 1.54 g (62%) of a white solid. m.p.: 155.0–155.8 °C (lit. 154–156 °C) [54]. ^{1}H NMR (200 MHz, $CDCl_3$) δ ppm: 3.89 (s, 3H, -OCH_3), 7.03 (d, *J* = 9.0 Hz, 2H, Ar-H), 7.47 (ddd, *J* = 7.7 Hz, 4.9 Hz and 1.2 Hz, 1H, Py-H), 7.90 (ddd, *J* = 7.9 Hz, 7.7 Hz and 1.7 Hz, 1H, Py-H), 8.16 (d, *J* = 9.0 Hz, 2H, Ar-H), 8.30 (ddd, *J* = 7.9 Hz, 1.2 Hz and 1.0 Hz, 1H, Py-H), 8.81 (ddd, *J* = 4.9 Hz, 1.7 Hz and 1.0 Hz, 1H, Py-H). ^{13}C NMR (50.3 MHz, $CDCl_3$) δ ppm: 55.42, 114.43,

115.99, 123.05, 125.58, 129.06, 137.13, 143.69, 150.19, 162.53, 163.36, 165.48. Q-TOF/MS for $C_{14}H_{12}N_3O_2$ $[M^+H]^+$: Calculated: 254.0924; Found: 254.0928.

The precursor $[\{(\eta^6\text{-}C_6H_6)ClRu\}_2Cl_2]$ was synthesized following the procedure described in the literature [55, 56].

Synthesis of compounds 1a, 1b, 3a and 3b (neutral complexes)

In a 100-mL round-bottom flask, 0.1 g (0.2 mmol) of the precursor $[\{(\eta^6\text{-}C_6H_6)ClRu\}_2Cl_2]$ was mixed with 0.15 g (0.1 mmol) of the ligand in 20 mL THF. Next, the reaction mixture was heated under reflux for 6 h. Then, the mixture was cooled to room temperature. After that, 10 mL ethanol was added to precipitate the product, which was kept under refrigeration for 12 h. Finally, the product was filtered and washed with ethanol and THF, and dried under vacuum in a desiccator with anhydrous calcium chloride. For further purification, the compounds were dissolved in dichloromethane with the minimum volume needed for total solubilization, and then filtered through Celite. In this step, the excess of the ruthenium precursor present in the mixture was separated in the Celite. The filtered solution was left to allow partial evaporation of the dichloromethane and concentration of the mixture. The mixture was filtered through Celite again to remove additional precipitated precursor. The procedure was repeated once more. After that, the dichloromethane was totally evaporated and the mixture suspended in THF and filtered in a sintered glass filter. In this step, the product was separated from the solution containing the excess of the free ligand. The product was washed with THF and dried under vacuum.

Compound 1a: Orange solid. Yield 17%. CHN: $RuON_3Cl_2C_{29}H_{39}.H_2O$ experimental (calculated): %C: 55.6 (54.8), %H: 6.3 (6.5), and %N: 7.0 (6.6). Purity 99.94%. ^{1}H NMR: (200 MHz, 30 °C, $CDCl_3$, TMS) δ ppm: 0.88 (3H, H_1), 1.27 (16H, H_2), 1.48 (2H, H_3), 1.83 (2H, H_4), 4.08 (2H, H_5), 5.70 (6H, H_{10}), 7.03 (2H, $H_{6,6'}$), 7.67 (2H, $H_{8,8'}$), 7.97 (2H, $H_{7,7'}$),

9.21 (2H, $H_{9,9'}$). IR (KBr) (ν_{max} cm^{-1}): 3066, 2924 and 2853 (ν_{CH}), 1599 (ν_{CC}), 1497 and 1412 (ν_{CN}), 1254 (ν_{asCOC}), 1146 (δ_{CH}), 1015 (ν_{sCOC}), 832 (π_{CH}) and 564 (π_{CC}).

Compound 1b: Yellow solid. Yield 21%. CHN: $RuON_3Cl_2C_{18}H_{17}.H_2O$ experimental (calculated): %C: 45.6 (44.9), %H: 3.7 (3.9), and %N: 8.7 (8.7). Purity 99.94%. ^{1}H NMR: (200 MHz, 30 °C, $CDCl_3$, TMS) δ ppm: 3.93 (3H, H_1), 5.69 (6H, H_{10}), 7.04 (2H, $H_{6,6'}$), 7.68 (2H, $H_{8,8'}$), 7.99 (2H, $H_{7,7'}$), 9.22 (2H, $H_{9,9'}$). IR (KBr) (ν_{max} cm^{-1}): 3066 (ν_{CH}), 1599 (ν_{CC}), 1499 and 1410 (ν_{CN}), 1258 (ν_{asCOC}), 1144 (δ_{CH}), 1023 (ν_{sCOC}), 832 (π_{CH}) and 562 (π_{CC}).

Compound 3a: Yellow solid. Yield 35%. CHN: $RuO_2N_3Cl_2C_{31}H_{39}.H_2O$ experimental (calculated): %C: 56.1 (55.1), %H: 6.0 (6.1), and %N: 6.4 (6.2). Purity 99.92%. ^{1}H NMR: (200 MHz, 30 °C, $CDCl_3$, TMS) δ ppm: 0.88 (3H, H_1), 1.27 (16H, H_2), 1.48 (2H, H_3), 1.83 (2H, H_4), 4.05 (2H, H_5), 5.72 (6H, H_{10}), 7.05 (2H, $H_{6,6'}$), 7.99 (2H, $H_{8,8'}$), 8.08 (2H, $H_{7,7'}$), 9.32 (2H, $H_{9,9'}$). IR (KBr) (ν_{max} cm^{-1}): 3065, 2928 and 2853 (ν_{CH}), 1613 (ν_{CC}), 1495 and 1420 (ν_{CN}), 1258 (ν_{asCOC}), 1173 (δ_{CH}), 1030 (ν_{sCOC}), 843 (π_{CH}).

Compound 3b: Brown solid. Yield 4%. CHN: $RuO_2N_3Cl_2C_{20}H_{17}.H_2O$ experimental (calculated): %C: 37.3 (46.0), %H: 2.7 (3.6), and %N: 7.2 (8.0). Purity 99.12%. ^{1}H NMR: (200 MHz, 30 °C, $CDCl_3$, TMS) δ ppm: 3.92 (3H, H_1), 5.72 (6H, H_{10}), 7.07 (2H, $H_{6,6'}$), 7.81 (2H, $H_{8,8'}$), 8.09 (2H, $H_{7,7'}$), 9.32 (2H, $H_{9,9'}$). IR (KBr) (ν_{max} cm^{-1}): 3069 (ν_{CH}), 1613 (ν_{CC}), 1495 and 1422 (ν_{CN}), 1262 (ν_{asCOC}), 1179 (δ_{CH}), 1025 (ν_{sCOC}), 840 (π_{CH}).

Synthesis of compounds 2a, 2b, 4a and 4b (positive charged complexes)

In a 100-mL Schlenk flask, 0.1 g (0.2 mmol) of the precursor $[\{(\eta^6\text{-}C_6H_6)ClRu\}_2Cl_2]$ was mixed in 20 mL methanol. Then, the ligand of interest (added in a stoichiometric amount, 2:1)

was dissolved in 10 mL methanol and slowly added to the reaction mixture. The solution was stirred for 4 h at room temperature and protected from light (with the exception of compound **4a**, which was stirred for 18 h at 120 °C. After that, the solvent was removed by rotoevaporation to approximately 1 mL and NH_4PF_6 in a methanol solution was added in excess. The mixture was kept under refrigeration for 24 h. Finally, the product was filtered and washed with methanol and ether, and dried under vacuum in a desiccator with anhydrous calcium chloride. It was only necessary to purify compound **2b**.

Compound 2a: Brown solid. Yield 79%. CHN $RuON_3ClC_{29}H_{39}PF_6.H_2O$ experimental (calculated): %C: 45.5 (46.7), %H: 5.6 (5.5), and %N: 5.9 (5.6). Purity 99.95%. ^{1}H NMR: (200 MHz, 30 °C, $CDCl_3$, TMS) δ ppm:0.89 (3H, H_1), 1.28 (16H, H_2), 1.48 (2H, H_3) 1.87 (2H, H_4), 4.14 (2H, H_5), 6.05 (6H, H_{10}), 7.09 (2H, $H_{6,6'}$), 7.73 (1H, H_9), 8.21 (2H, $H_{7,7'}$), 8.50 (d, 1H, H_8 and t, 1H, $H_{8'}$), 9.30 (1H, $H_{9'}$). IR (KBr) (ν_{max} cm^{-1}): 3109, 2924 and 2851 (ν_{CH}), 1597 (ν_{CC}), 1499 and 1409 (ν_{CN}), 1260 (ν_{asCOC}), 1150 (δ_{CH}), 1020 (ν_{sCOC}), 838 (ν_{PF}) and 560 (π_{CC}). ESI/MS for $M^+[RuON_3ClC_{29}H_{39}]^+$: Calculated: 582.18; found: m/z 582.34.

Compound 2b: Brown solid. Yield 25%. CHN $RuON_3ClC_{18}H_{17}PF_6.H_2O$ experimental (calculated): %C: 37.0 (36.6), %H: 3.2 (3.2), and %N: 6.9 (7.1). Purity 99.96%. ^{1}H NMR: (200 MHz, 30 °C, $CDCl_3$, TMS) δ ppm: 3.81 (3H, H_1), 6.07 (6H, H_{10}), 7.56 (2H, $H_{6,6'}$), 7.76 (1H, H_9), 8.19 (2H, $H_{7,7'}$), 8.54 (2H, $H_{8,8'}$), 8.92 (1H, $H_{9'}$). IR (KBr) (ν_{max} cm^{-1}): 3094 (ν_{CH}), 1596 (ν_{CC}), 1466 and 1370 (ν_{CN}), 1262 (ν_{asCOC}), 1154 (δ_{CH}), 1027 (ν_{sCOC}), 832 (ν_{PF}) and 558 (π_{CC}). ESI/MS for $M^+[RuON_3ClC_{18}H_{17}]^+$: Calculated: 427.88; found: m/z 428.09.

Compound 4a: Green solid. Yield 79%. CHN $RuO_2N_3ClC_{31}H_{39}PF_6.H_2O$ experimental (calculated): %C: 45.3 (47.4), %H: 5.0 (5.3), and %N: 5.8 (5.3). Purity 99.87%. ^{1}H NMR:

(200 MHz, 30 °C, CDCl3, TMS) δ ppm:0.89 (3H, H_1), 1.28 (16H, H_2), 1.48 (2H, H_3), 1.87 (2H, H_4), 4.07 (2H, H_5), 6.12 (6H, H_{10}), 7.06 (2H, $H_{6,6'}$), 7.73 (1H, H_9), 8.09 (4H, $H_{7,7',8,8'}$), 9.38 (1H, $H_{9'}$). IR (KBr) (ν_{max} cm^{-1}): 3094, 2923 and 2853 (ν_{CH}), 1609 (ν_{CC}), 1499 and 1438 (ν_{CN}), 1262 (ν_{asCOC}), 1179 (δ_{CH}), 1025 (ν_{sCOC}), 838 (ν_{PF}). ESI/MS for $M^+[RuO_2N_3ClC_{31}H_{39}]^+$: Calculated: 622.20; found: m/z 622.31.

Compound 4b: Green solid. Yield 77%. CHN $RuO_2N_3ClC_{20}H_{17}PF_6.H_2O$ experimental (calculated): %C: 37.2 (38.0), %H: 3.1 (3.0), and %N: 6.8 (6.6). Purity 99.93%. ^1H NMR: (200 MHz, 30 °C, $CDCl_3$, TMS) δ ppm: 3.94 (3H, H_1), 6.15 (6H, H_{10}), 7.09 (2H, $H_{6,6'}$), 7.75 (1H, H_9), 8.11 (4H, $H_{7,7,8,8'}$), 9.35 (1H, $H_{9'}$). IR (KBr) (ν_{max} cm^{-1}): 3094 (ν_{CH}), 1609 (ν_{CC}), 1500 and 1420 (ν_{CN}), 1265 (ν_{asCOC}), 1181 (δ_{CH}), 1021 (ν_{sCOC}), 836 (ν_{PF}). ESI/MS for $M^+[RuO_2N_3ClC_{20}H_{17}]^+$: Calculated: 467.90; found: m/z 468.16.

Biology

Cell Cultures. The human embryonic kidney HEK293 cell lines transfected with *ABCG2* (HEK293 *ABCG2*), mouse embryonic fibroblast wild-type (NIH3T3) and *P-gp*-overexpressing (NIH3T3 *ABCB1*), as well as the human glioblastoma T98G, U87MG and U251 cell lines, were maintained in Dulbecco's modified Eagle's medium (DMEM high glucose) (Sigma-Aldrich), supplemented with 10% fetal bovine serum (FBS), 1% penicillin/streptomycin, and supplemented with 0.75 $mg{\cdot}mL^{-1}$ G418 (HEK293 *ABCG2*), or 60 $ng{\cdot}mL^{-1}$ colchicin (NIH3T3 *P-gp*). The mammalian fibroblast baby hamster kidney 21 cells (BHK21) and MRP1-overexpressing cells (BHK21 *MRP1*) were maintained in Dulbecco's modified Eagle's medium (DMEM/F12), supplemented with 5% fetal bovine serum (FBS), 1% penicillin/streptomycin, and supplemented for BHK21 *MRP1* with 0.1 $mg{\cdot}mL^{-1}$ methotrexate.

Cytotoxicity Assays. Different cell lines were seeded into 96-well culture plates at an appropriate concentration to allow a log-linear growth for 3 d. Twenty-four hours after plating, the cells were treated with increasing concentrations of 0.1 to 100 $\mu mol \cdot L^{-1}$ compounds for 72 h, at 37 °C under 5% CO_2. Cell viability was then evaluated with an MTT colorimetric assay [57]. Control experiments were performed with DMEM high glucose containing 0.1% DMSO (v/v). The results were expressed as percentage of viable cells *versus* initial control cells, taken as 100%.

Flow cytometric analysis. Human tumor cells (6×10^4 cells/well) were incubated in 12-well plates (24 h, 37 °C). The cells were then treated with 25 and 100 $\mu mol \cdot L^{-1}$ η^6-areneruthenium(II) compounds for 72 h. After centrifugation, the pellet was washed twice with PBSA and incubated with a cold staining solution of 50 $\mu g \cdot mL^{-1}$ propidium iodide, 0.1% Triton X-100, 0.1% sodium citrate, and 0.2 $mg \cdot mL^{-1}$ RNAse A (30 min, in the dark) [58]. The samples were run in a FACSCalibur System, and the DNA histograms obtained were analyzed to measure their relative DNA content (characterizing G1, S, G2 phase distributions and the proportion of sub-G1 hypodiploid cells), using Win MDI 2.9 software (developed by Joseph Trotter).

Statistical analysis. Mean ± SD results were submitted to analysis of variance (one-way ANOVA) using the GraphPad Prism 5 program. Values of $p \leq 0.05$ were considered statistically significant.

Acknowledgments

The authors thank the Ligue Nationale Contre le Cancer (Equipe Labellisée 2014) for financial support. Amanda Pires thanks CNPq and the Science Without Borders Program 2014-3/ 2014-5. Jaqueline Pazinato thanks CAPES and the Overseas Sandwich Doctorate Program 6738/14-9. The authors also thank Elizangela Cavazzini Cesca for the NMR analyses and discussions, and CEBIME-UFSC for the HR-MS analysis.

REFERENCES

1. *M.E. Salacz, K.R. Watson, D.A. Schomas, Glioblastoma: Part I. Current state of affairs,* J. Missouri State Med. Assoc. *108 (2011) 187–194.*

2. *M. Jhanwar-Uniyal, et al., Glioblastoma: Molecular Pathways, Stem Cells and Therapeutic Targets, Cancers 7 (2015) 538.*

3. *F.B. Furnari, et al., Malignant astrocytic glioma: genetics, biology, and paths to treatment, Genes Dev. 21 (2007) 2683–2710.*

4. *E.G. Van Meir, et al., Exciting new advances in neuro-oncology: the avenue to a cure for malignant glioma*, CA Cancer J. Clin. *60 (2010) 166–193.*

5. *A. Nowacek, H.E. Gendelman, NanoART, neuroAIDS and CNS drug delivery. Nanomedicine 4 (2009) 557–574.*

6. *G. Szakacs, et al., Targeting multidrug resistance in cancer,* Nat. Rev. Drug Discovery *5 (2006) 219–234.*

7. *Z. Chen, et al., Mammalian drug efflux transporters of the ATP binding cassette (ABC) family in multidrug resistance: A review of the past decade, Cancer Lett. 370 (2016) 153–164.*

8. P. Borst, A.H. Schinkel, P-glycoprotein ABCB1: a major player in drug handling by mammals, J. Clin. Invest. 123 (2013) 4131–4133.

9. M.L.H. Vlaming, J.S. Lagas, A.H. Schinkel, Physiological and pharmacological roles of ABCG2 (BCRP): Recent findings in Abcg2 knockout mice, Adv. Drug Delivery Rev. 61 (2009) 14–25.

10. K.M. Pluchino, et al., Collateral sensitivity as a strategy against cancer multidrug resistance, Drug Resist. Updat. 15 (2012) 98–105.

11. A. Tamaki, et al., The controversial role of ABC transporters in clinical oncology, Essays Biochem. 50 (2011) 209–232.

12. M. Dean, Y. Hamon, G. Chimini, The human ATP-binding cassette (ABC) transporter superfamily, J. Lipid Res. 42 (2001) 1007–1017.

13. G. Chang, Multidrug resistance ABC transporters, FEBS Lett. 555 (2003) 102–105.

14. R. Doshi, et al., The choreography of multidrug export, Biochem. Soc. Trans. 39 (2011) 807–811.

15. O. Bähr, et al., P-Glycoprotein and Multidrug Resistance-associated Protein Mediate Specific Patterns of Multidrug Resistance in Malignant Glioma Cell Lines, but not in Primary Glioma Cells, Brain Pathol. 13 (2003) 482–494.

16. A.M. Bleau, et al., The ABCG2 resistance network of glioblastoma, Cell Cycle 8 (2005) 2937–2945.

17. C. Caratozzolo, et al., Expression of drug resistance proteins Pgp, MRP1, MRP3, MRP5 and GST-pi in human glioma, J. Neurooncol. 74 (2005) 113–121.

18. B. Benyahia, et al., Multidrug resistance-associated protein MRP1 expression in human gliomas: chemosensitization to vincristine and etoposide by indomethacin in human glioma cell lines overexpressing MRP1, J. Neurooncol. 66 (2004) 65–70.

19. K.B. Pointer, et al., Glioblastoma cancer stem cells: Biomarker and therapeutic advances, Neurochem. Int. 71 (2014) 1–7.

20. G. Minniti, et al., Chemotherapy for Glioblastoma: Current Treatment and Future Perspectives for Cytotoxic and Targeted Agents, Anticancer Res. 29 (2009) 5171–5184.

21. S. D'Atri, et al., Attenuation of O(6)-methylguanine-DNA methyltransferase activity and mRNA levels by cisplatin and temozolomide in jurkat cells, J. Pharmacol. Exp. Ther. *294 (2000) 664–671.*

22. A.A. Brandes, et al., First-Line Chemotherapy With Cisplatin Plus Fractionated Temozolomide in Recurrent Glioblastoma Multiforme: A Phase II Study of the Gruppo Italiano Cooperativo di Neuro-Oncologia, J. Clin. Oncol. 22 (2004) 1598–1604.

23. F. Zustovich, et al., A Phase II Study of Cisplatin and Temozolomide in Heavily Pre-treated Patients with Temozolomide-refractory High-grade Malignant Glioma, Anticancer Res. 29 (2009) 4275–4279.

24. D. Jones, L. Pratt, G. Wilkinson, -Cyclohexadienyl compounds of manganese, rhenium, iron, and ruthenium, J. Chem. Soc. (1962) 4458.

25. C.S. Allardyce, et al., Synthesis and characterization of some water soluble ruthenium(II)/arene complexes and an investigation of their antibiotic and antiviral properties, J. Organomet. Chem. 668 (2003) 35–42.

26. Y.K. Yan, M. Melchart, A. Habtemariam, P.J. Sadler, Organometallic chemistry, biology and medicine: ruthenium arene anticancer complexes, Chem. Commun. 38 (2005) 4764–4776.

27. S.J. Dougan, M. Melchart, A. Habtemariam, S. Parsons, P. J. Sadler, Phenylazo-pyridine and Phenylazo-pyrazole Chlorido Ruthenium(II) Arene Complexes: Arene Loss, Aquation, and Cancer Cell Cytotoxicity, Inorg. Chem. 45 (2006) 10882–10894.

28. C. Scolaro, et al., In vitro and in vivo evaluation of ruthenium(II)-arene PTA complexes, J. Med. Chem. 48 (2005) 4161–4171.

29. C.S. Allardyce, et al., [Ru([small-eta]-cymene)Cl(pta)] (pta=1,3,5-triaza-7-phosphatricyclo-[3.3.1.1]decane): a water soluble compound that exhibits pH dependent DNA binding providing selectivity for diseased cells, Chem. Commun. 15 (2001) 1396–1397.

30. G. Suss-Fink, Arene ruthenium complexes as anticancer agents, Dalton Trans. 39 (2010) 1673–1688.

31. W.H. Ang, et al., Development of Organometallic Ruthenium−Arene Anticancer Drugs That Resist Hydrolysis, Inorg. Chem. 45 (2006) 9006–9013.

32. P.J. Dyson, Systematic Design of a Targeted Organometallic Antitumour Drug in Pre-clinical Development, CHIMIA Int. J. Chem. 61 (2007) 698–703.

33. S.J. Dougan, et al., Catalytic organometallic anticancer complexes, Proc. Natl. Acad. Sci. U.S.A. 105 (2008) 11628–11633.

34. M.K.M. Subarkhan, R. Ramesh, Ruthenium(II) arene complexes containing benzhydrazone ligands: synthesis, structure and antiproliferative activity, Inorg. Chem. Front. 3 (2016) 1245–1255.

35. C.W. Haigh, R.B. Mallion, Ring current theories in nuclear magnetic resonance, Prog. Nucl. Magn. Reson. Spectrosc. 13 (1979) 303–344.

36. L. Pazderski, et al., ^{1}H, ^{13}C and ^{15}N NMR coordination shifts in gold(III), cobalt(III), rhodium(III) chloride complexes with pyridine, 2,2 -bipyridine and 1,10-phenanthroline, Magn. Reson. Chem. 45 (2007) 24–36.

37. J.L. Sadler, A.J. Bard, The Electrochemical Reduction of Aromatic Azo Compound, J. Am. Chem. Soc. 1968 (1979) 90.

38. S. Goswami, R. Mukherjee, A. Chakravorty, Chemistry of Ruthenium. 12.' Reactions of Bidentate Ligands with Diaquobis[2-(arylazo)pyridine]ruthenium(II) Cation. Stereoretentive Synthesis of Tris Chelates and Their Characterization: Metal Oxidation, Ligand Reduction, and Spectroelectrochemical Correlation, Inorg. Chem. 22 (1983) 2825–2832.

39. J. Palmucci, et al., Synthesis, Structure, and Anticancer Activity of Arene−Ruthenium(II) Complexes with Acylpyrazolones Bearing Aliphatic Groups in the Acyl Moiety, Inorg. Chem. 55 (2016) 11770−11781.

40. R.J. Kathawala, et al., The modulation of ABC transporter-mediated multidrug resistance in cancer: A review of the past decade, Drug Resist. Update. 18 (2015) 1–17.

41. S. Spiegl-Kreinecker, et al., Expression and Functional Activity of the ABC-transporter Proteins P-glycoprotein and Multidrug-resistance Protein 1 in Human Brain Tumor Cells and Astrocytes, J. Neurooncol. 57 (2002) 27–36.

42. A. Tivnan, et al., Inhibition of multidrug resistance protein 1 (MRP1) improves chemotherapy drug response in primary and recurrent glioblastoma multiforme, Front. Neurosci. 9 (2015) 218.

43. D. Keppler, Export pumps for glutathione S-conjugates, Free Radic. Biol. Med. 27 (1999) 985–991.

44. S.P. Cole, R.G. Deeley, Transport of glutathione and glutathione conjugates by MRP1, Trends Pharmacol. Sci. *27 (2006) 438–446.*

45. F.Q. Schafer, G.R. Buettner, Redox environment of the cell as viewed through the redox state of the glutathione disulfide/glutathione couple, Free Radic. Biol. Med. 30 (2001) 1191–1212.

46. D. Montero, et al., Intracellular glutathione pools are heterogeneously concentrated, Redox Biol. 1 (2013) 508–513.

47. K.P. Naidek, et al., Ruthenium Acetate Cluster Amphiphiles and Their Langmuir–Blodgett Films for Electrochromic Switching Devices, Eur. J. Inorg. Chem. 7 (2014) 1150–1157.

48. V.S. Padalkar, et al., Efficient Synthesis of 3-Substituted 1,2,4-Triazolo[4,3-a]pyridine by [Bis(Trifluroacetoxy)iodo]benzene-Catalyzed Oxidative Intramolecular Cyclization of Heterocyclic Hydrazones, Synthetic Commun. 41 (2011) 925–938.

49. E. Westphal, et al., Room temperature columnar liquid crystalline phases of luminescent non-symmetric star-shaped molecules containing two 1,3,4-oxadiazole units, J. Mater. Chem. C. 1 (2013) 8011–8022.

50. E.C. Taylor, C.P. Tseng, J.B. Rampal, Conversion of a primary amino group into a nitroso group. Synthesis of nitroso-substituted heterocycles, J. Org. Chem. 47 (1982) 552–555.

51. E. Westphal, et al., Pyridinium and imidazolium 1,3,4-oxadiazole ionic liquid crystals: a thermal and photophysical systematic investigation, RSC Adv. 3 (2013) 6442–6454.

52. M. Dabiri, et al., A facile procedure for the one-pot synthesis of unsymmetrical 2,5-disubstituted 1,3,4-oxadiazoles, Tetrahedron Lett. 47 (2006) 6983–6986.

53. A. Facchetti, et al., Novel coordinating motifs for lanthanide(iii) ions based on 5-(2-pyridyl)tetrazole and 5-(2-pyridyl-1-oxide)tetrazole. Potential new contrast agents, Chem. Commun. 15 (2004) 1770–1771.

54. Y. Liu, et al., A novel terbium complex using oxadiazole derivative as a neutral ligand: Synthesis and properties, Chin. Chem. Lett. 18 (2007) 573–576.

55. M.A. Bennett, T.W. Matheson, A simple preparation of bis-arene-ruthenium cationic complexes, including those containing different arenes, J. Organomet. Chem. 175 (1979) 87–93.

56. R.A. Zelonka, M.C. Baird, Benzene Complexes of Ruthenium(II), Can. J. Chem. 50 (1972) 3063–3072.

57. T. Mosmann, Rapid colorimetric assay for cellular growth and survival: Application to proliferation and cytotoxicity assays, J. Immunol. Meth. 65 (1983): 55–63.

58. C. Riccardi, I. Nicoletti, Analysis of apoptosis by propidium iodide staining and flow cytometry, Nature Protocols. 1 (2006) 1458–1461.

Graphical Abstract

A series of amphiphilic η^6-areneruthenium(II) compounds were synthesized, characterized, and their biological activity evaluated in human glioblastoma cell lines. Compound recognition by ABC transporters (P-gp, MRP1, and ABCG2) was investigated. Results evidenced that one of the cationic phenylazo-based η^6-areneruthenium(II) compound was cytotoxic for all human glioblastoma cell lines tested, despite its transport by the three multidrug efflux proteins.

Figure captions

Scheme 1. Precursor $[\{(\eta^6\text{-}C_6H_6)ClRu\}_2Cl_2]$ at center and the amphiphilic complexes. Group I: compounds **1a, 1b, 2a** and **2b** with the **L1a, L1b, L2a** and **L2b** ligands, and group II: compounds **3a, 3b, 4a** and **4b** with the **L3a, L3b, L4a** and **L4b** ligands. **L1a =** 4-(4-dodecyloxyphenylazo)pyridine, **L1b** = 4-(4-methoxyphenylazo)pyridine, **L2a** = 2-(4-dodecyloxyphenylazo)pyridine, **L2b** = 2-(4-methoxyphenylazo)pyridine, **L3a** = 2-(4-dodecyloxyphenyl)-5-(4-pyridyl)-1,3,4-oxadiazole, **L3b** = 2-(4-methoxyphenyl)-5-(4-pyridyl)-1,3,4-oxadiazole, **L4a** = 2-(4-dodecyloxyphenyl)-5-(2-pyridyl)-1,3,4-oxadiazole, **L4b** = 2-(4-methoxyphenyl)-5-(2-pyridyl)-1,3,4-oxadiazole.

Figure 1. Cyclic voltammograms of compounds (A) **2a** and (B) **2b** in dichloromethane, and compounds (C) **2a** and (D) **2b** in acetonitrile. $TBAClO_4$ 0.1 $mol{\cdot}L^{-1}$. Scan rates = 5–100 $mV{\cdot}s^{-1}$ (labels indicated on the graph).

Figure 2. Effect of the compounds on cell-cycle progression in glioblastoma cells. T98G cells were treated with different η^6-areneruthenium complexes at (A) 25 and (B) 100 $\mu mol \cdot L^{-1}$ for 72 h. Cellular DNA was stained with propidium iodide and flow-cytometry analysis was performed to analyze the cell cycle distribution. (C) Percentage of fragmented DNA content after the compound treatment. *** for $p < 0.001$.

Figure 3. Cytotoxic effect of compound **2b** in transfected cells overexpressing multidrug ABC transporters. The cells were treated with several concentrations of compound **2b** for 72 h with or without specific inhibitors of the ABC transporters. The cytotoxicity was evaluated by MTT assays (see Experimental Section): (A) (square) NIH 3T3, (circle) NIH 3T3-*P-gp*, (up-triangle) NIH 3T3-*P-gp* with GF12018/elacridar (at 1 $\mu mol \cdot L^{-1}$ concentration); (B) (square) HEK293, (circle) HEK293-*ABCG2*, (up-triangle) HEK293-*ABCG2* with Ko143 (at 1 $\mu mol \cdot L^{-1}$ concentration); (C) (square) BHK21, (circle) BHK21-*MRP1*, (up-triangle) BHK21-*MRP1mutant*.

Figure 4. UV-vis spectra involved in the interaction of compound **2b** with GSH experiments. UV-vis spectra of (solid black line) GSH; (dashed black line) GSH solution treated with an equivalent of H_2O_2; (blue line) GSH with compound **2b** solution after interaction for 10 s and (red line) after 1 h. The concentrations used were 10 $mmol \cdot L^{-1}$ GSH, 10 $mmol \cdot L^{-1}$ H_2O_2 and 100 $\mu mol \cdot L^{-1}$ compound **2b**.

Figure 5. Cytotoxic effects of compound **2b** on glioblastoma T98G cells. Cells were treated with compound **2b** at several concentrations for 72 h, with or without specific inhibitors of ABC transporters. The cytotoxicity was determined by MTT assays: (square) compound **2b** (at 0–20 $\mu mol \cdot L^{-1}$); (up-triangle) compound **2b** with MBLII141 (at 2 $\mu mol \cdot L^{-1}$); (circle)

compound **2b** with verapamil (at 10 µmol·L^{-1}); (down-triangle) compound **2b** with Ko143 (at 2 µmol·L^{-1}); (star) compound **2b** with GF120918 (at 2 µmol·L^{-1}).

Scheme 2. Synthetic route of the dodecyloxy- pyridine derivative ligands. *Reagents*: *i*) $NH_2NH_2.H_2O$ (65%); *ii*) hydroquinone, H_2SO_4, H_2O; *iii*) *n*-$C_{12}H_{25}Br$, K_2CO_3, butanone; *iv*) $SOCl_2$, DMF; *v*) anhydrous pyridine; v*i*) DCC, DMAP, anhydrous toluene.

Scheme 3. Synthetic route of the methoxy- pyridine derivative ligands. *Reagents*: *i*) acetone, CH_3I, K_2CO_3; *ii*) DMF, NaN_3, NH_4Cl; *iii*) $SOCl_2$, DMF; i*v*) anhydrous pyridine.

Tables

Table 1. Selected data obtained by ^{1}H-NMR for the η^6-areneruthenium(II) compounds and free ligands in $CDCl_3$

Compounds	**δ(ppm) H_α py**	**δ(ppm) H_β py**	**Free ligands**	**δ(ppm) H_α py**	**δ(ppm) H_β py**
1a	9.21	7.67	**L1a**	8.78	7.72
1b	9.22	7.68	**L1b**	8.78	7.67
2a	9.30	7.73	**L2a**	8.71	7.36
2b	8.92	7.76	**L2b**	8.70	7.37
3a	9.32	7.99	**L3a**	8.82	7.97
3b	9.32	7.81	**L3b**	8.83	7.97
4a	9.38	7.72	**L4a**	8.80	7.45
4b	9.35	7.75	**L4b**	8.81	7.47

Table 2. Cathodic peak potentials extracted from CV experiments for the group 1 η^6-areneruthenium(II) compounds

Compounds	E_{cp} **(V *vs SHE*)**		$E_{1/2}$ **(V *vs SHE*)**
L1a	–1.12*		–1.05*
L1b	–1.10*		–1.02*
L2a	–1.18*		
L2b	–1.20*		
1a	–0.80*		
1b	–0.83*		
2a	–0.15*	–0.22$^{\#}$	

2b	–0.19*	–0.21#

Data obtained in *CH_2Cl_2; in #CH_3CN.

Table 3. Cytotoxicity of the amphiphilic η^6-areneruthenium(II) compounds to the human glioblastoma cell lines U251, U87MG and T98G.

Compounds	IG_{50} (μmol·L^{-1})		
	U251	**U87MG**	**T98G**
Group I			
1a	22.09 ± 1.31	55.46 ± 8.05	71.91 ± 6.80
1b	56.00 ± 7.16	97.05 ± 1.70	31.04 ± 3.73
2a	5.92 ± 1.04	4.90 ± 0.98	5.5 ± 0.71
2b	8.03 ± 0.50	4.90 ± 1.08	24.77 ± 2.27
Group II			
3a	> 100	> 100	> 100
3b	> 100	> 100	> 100
4a	6.12 ± 1.56	5.66 ± 1.75	12.44 ± 3.49
4b	> 100	> 100	> 100

Notes: The IG_{50} values for the cytotoxicity of the compounds were determined using 10, 25, 50 and 100 μmol·L^{-1}, after 72 h of treatment by the MTT cell-survival method. Abbreviations: IG_{50}, half-maximal inhibitory growth concentration; MTT, 3-(4,5-dimethylthiazol-2-yl)-2,5-diphenyltetrazolium bromide.

Table 4. Cytotoxicity of η^6-areneruthenium(II) to transfected cells lines that overexpress multidrug ABC transporters.

Compounds	IG_{50} (µmol·L^{-1})					
	NIH 3T3	**NIH 3T3-*P-gp***	**HEK293**	**HEK293-*ABCG2***	**BHK21**	**BHK21-*MRP1***
			Group I			
1a	57.13 ± 1.25	64.82 ± 1.93	91.5 ± 9.19	85 ± 5.65	43.13 ± 3.83	20.20 ± 1.96
1b	51.27 ± 3.08	59.41 ± 4.44	43.66 ± 3.51	38.0 ± 5.29	30.67 ± 3.21	28.5 ± 5.06
2a	13.26 ± 1.13	16.44 ± 0.70	13.47 ± 0.45	13.30 ± 0.28	2.25 ± 0.27	0.80 ± 0.14
2b	11.61 ± 0.11	> 100	8.63 ± 0.48	16.10 ± 0.95	2.76 ± 0.49	4.36 ± 1.04
			Group II			
3a	> 100	> 100	> 100	> 100	> 100	> 100
3b	> 100	> 100	> 100	> 100	> 100	53.56 ± 6.83
4a	34.45 ± 0.54	65.06 ± 1.75	17.7 ± 2.00	8.55 ± 2.04	2.00 ± 0.34	1.85 ± 0.22
4b	> 100	> 100	> 100	> 100	> 100	> 100

Note: The respective IG_{50} values of the compounds are reported. Cells were treated with increasing concentrations of compounds for 72 h, before the cytotoxicity was evaluated by using the MTT assay.

Table 5. Resistance indexes displayed by compounds **2b** and **4a** to the multidrug transporters P-gp, ABCG2 and MRP1.

	Resistance index

Compounds	NIH 3T3-*P-gp*	HEK293-*ABCG2*	BHK21-*MRP1*
2b	8.6	1.8	1.6
4a	1.9	–	–

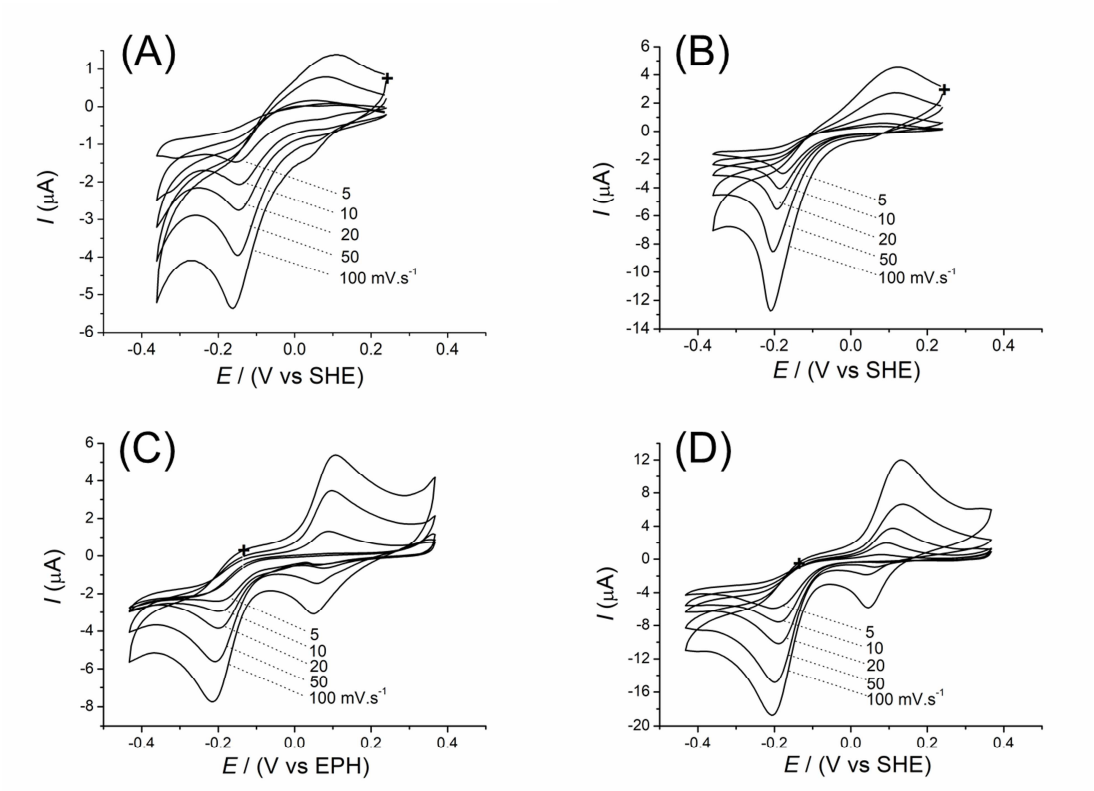
(A)
I (μA)
E / (V vs SHE)
5
10
20
50
100 mV.s-1
(B)
I (μA)
E / (V vs SHE)
5
10
20
50
100 mV.s-1
(C)
I (μA)
E / (V vs EPH)
5
10
20
50
100 mV.s-1
(D)
I (μA)
E / (V vs SHE)
5
10
20
50
100 mV.s-1

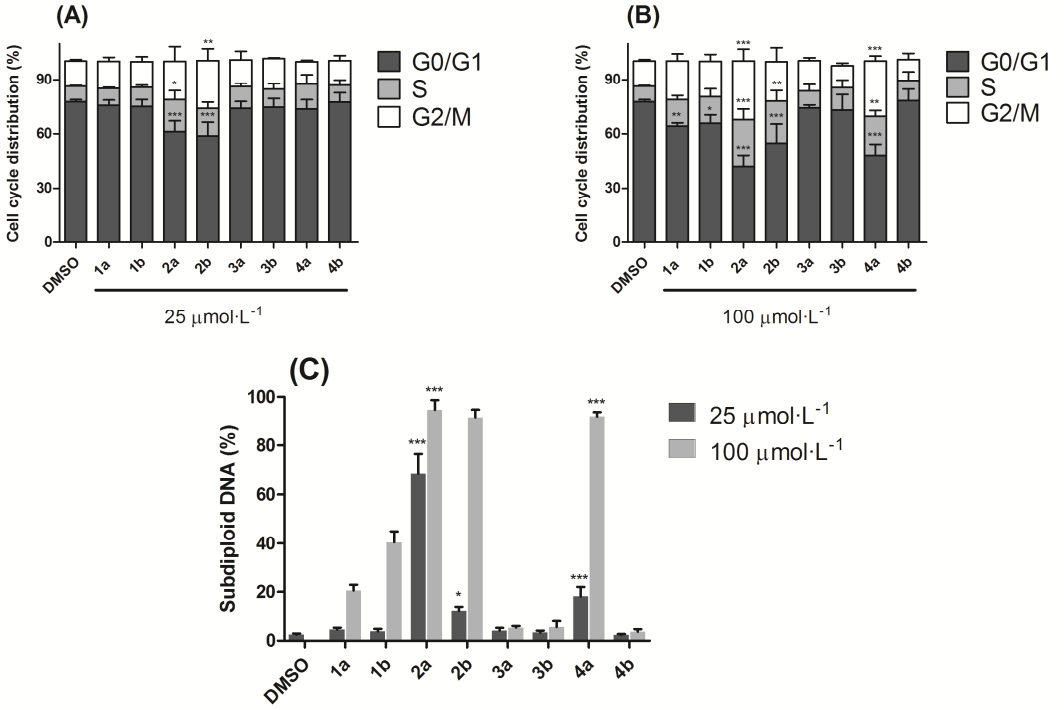

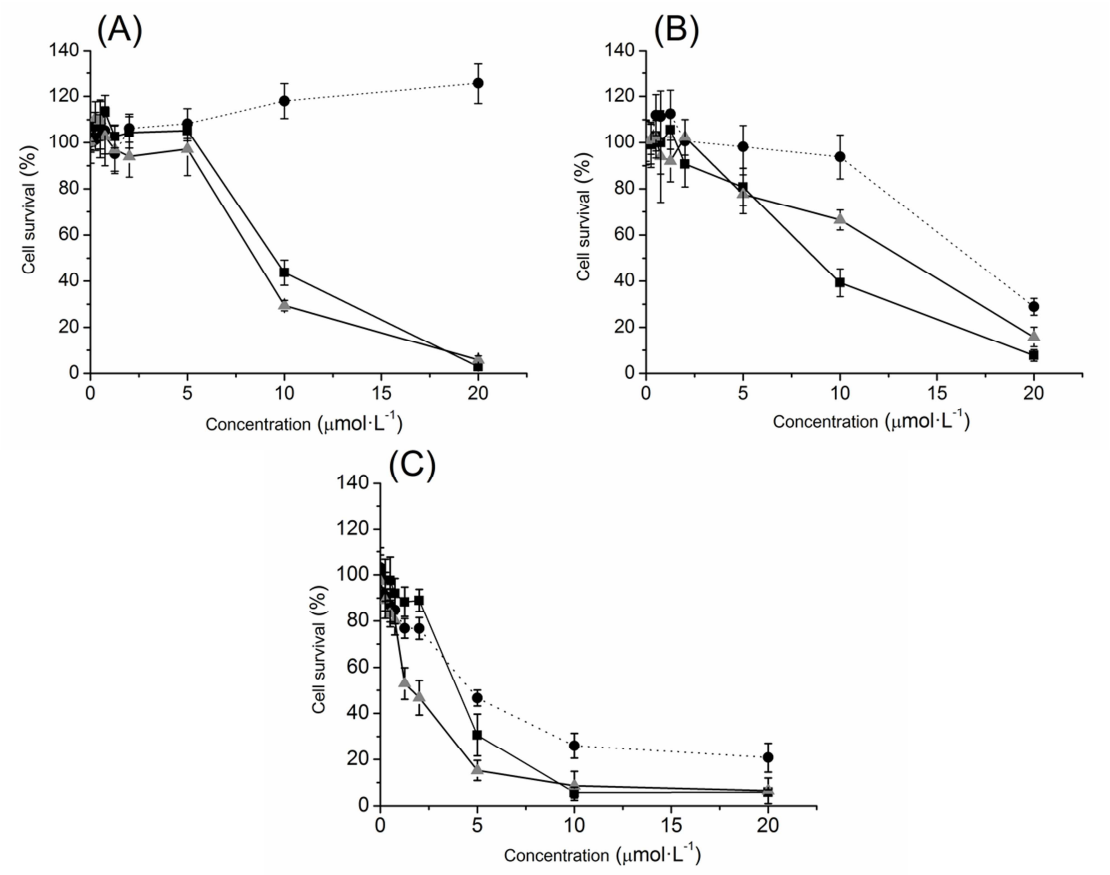

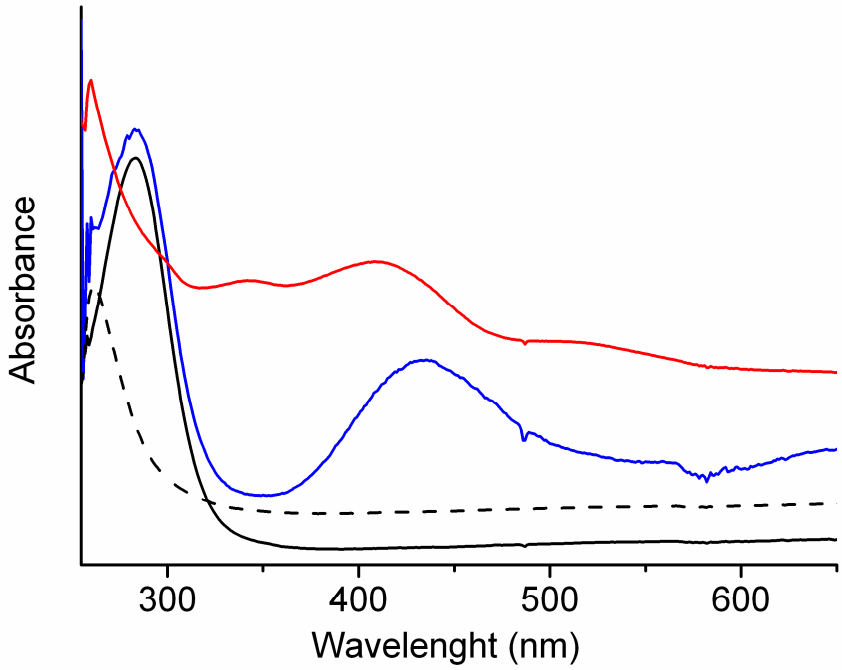

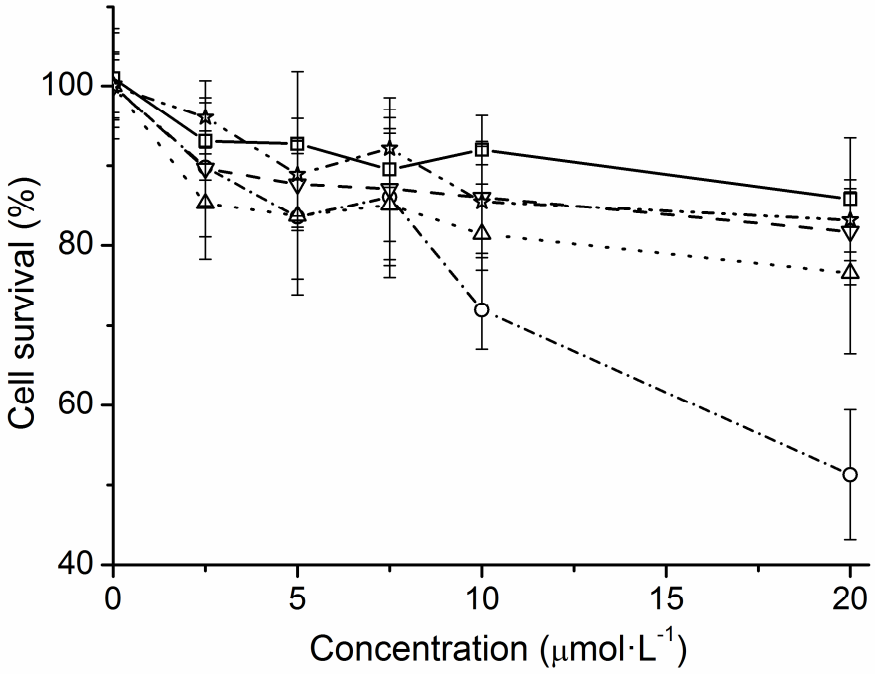

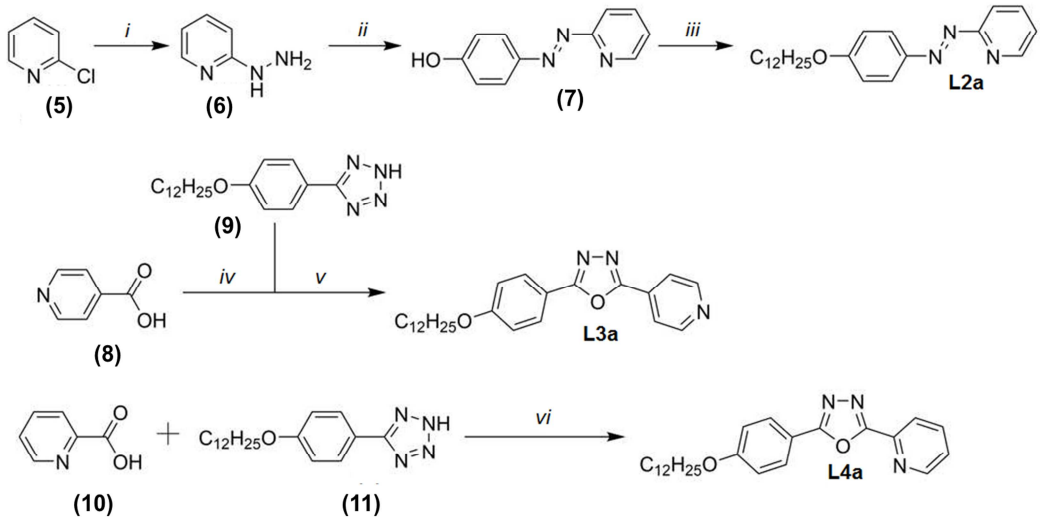

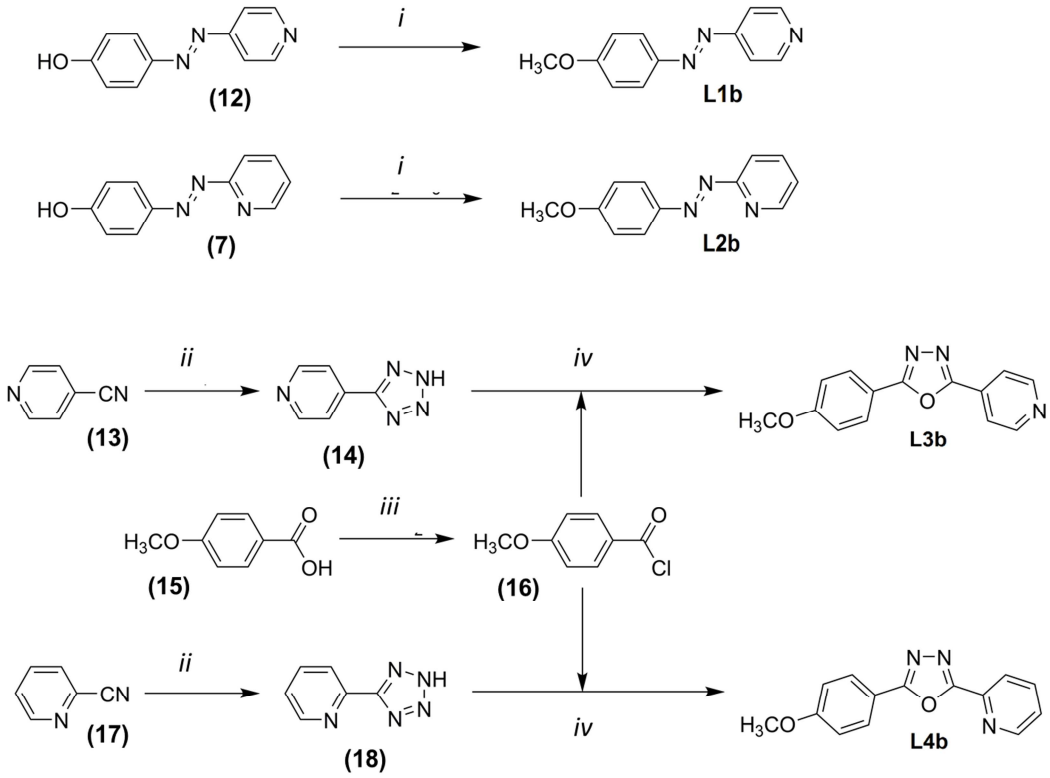

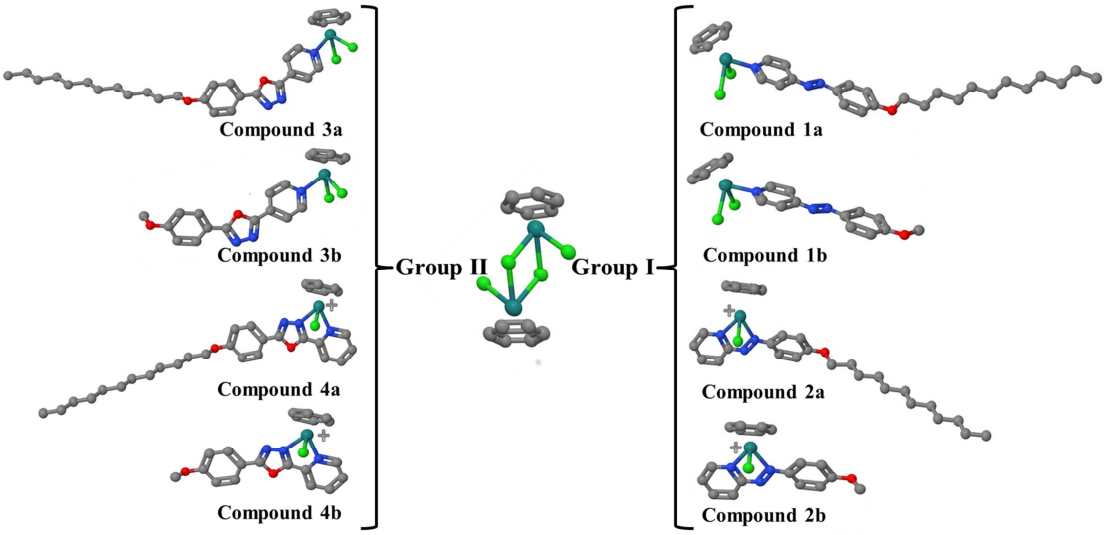

Highlights

- Two new series of amphiphilic η^6-areneruthenium(II) compounds were synthesized and characterized.

- The azo-derivative ruthenium complexes exhibited high cytotoxic activity on three human glioblastoma cell lines: U251, U87MG and T98G; and the cytotoxicity was attributed to alterations of cell-cycle progression and increased contents of fragmented DNA, suggesting an apoptotic mechanism.

- The azo-derivative compound **2b** was a substrate for the P-gp, ABCG2 and MRP1 protein transporters.

- The cytotoxicity of compound **2b** in the T98G cell line was highly increased by verapamil, revealing the involvement of multidrug ABC transporters.